Peer Review File

Universal and Scalable Synthesis of Photochromic Single-Atom Catalysts for Plastic Recycling

Corresponding Author: Professor Jinxing Chen

This file contains all reviewer reports in order by version, followed by all author rebuttals in order by version.

Version 0:

Reviewer comments:

Reviewer #1

(Remarks to the Author)
In this manuscript, the M1-TiO2 nanostructures with abundant M-O-Ti units are synthesized, and exhibit high efficiency in photochromic photothermal catalysis toward recycling waste polyesters. The authors have done extensive characterization of different single atoms and explained the synthesis process in detail from kinetic and thermodynamic limitation. However, it did not show significant advantages over other simple synthesis methods. At the same time, the precise sites and the mechanism in catalysis of single atoms are very vague. Taking into account the impact of the journal as well as the completeness and innovation of the current edition, it is not appropriate for the article to be accepted, the detail suggestions are as followed.
1. It has been reported that there are simpler ways to synthesize large quantities of single-atom/TiO2 catalysts, and the current system does not have a high single-atom loading. Therefore, the synthetic method does not show significant advantages.
2. The authors only considered the role of Fe in the generation of oxygen defects in the photochromism, whether Fe single atoms can act as catalytic sites was not considered and further theoretical and experimental evidence is needed to demonstrate this.
3. In the Figure 1f, the location marked by the authors is attributed to Ti, whether the material is attributed to oxygen defects or Ti defects?
4. The different valence states Ti achieves cycling during catalysis, and more experimental evidences are needed to prove.
5. In the photocatalytic process, the authors only considered the role of photogenerated electrons in photochromism. Also, electrons can catalyze the generation of oxide species. The authors need further experimental evidence to exclude this effect.
6. In order to highlight the advantages of single atoms in the catalytic process, the authors need to add further experiments related to Fe or FeOx species.
7. The intermediate species in the catalytic process require further experimental and theoretical evidences.
8. The catalytic time of 30 min is not sufficient, and further extension is required to further illustrate catalyst stability. And the catalyst needs to be further characterized after the reaction.
9. The authors need to add a comparison of activity relative to other reported catalysts.

Reviewer #2

(Remarks to the Author)
The research on the universal and scalable synthesis of single-atom catalysts and their application for plastic recycling are interesting. In this manuscript, the synthesis of supported M1-TiO2 single atom catalysts was claimed to be succeeded for about 20 different elements. The Fe1-TiO2 single atom catalyst was chosen as an example characterized by various techniques and applied to the photothermal catalysis of plastics including films, PET and so on. A lot of work had been done, but reorganization was needed. It can be resubmitted if the following questions could be carefully considered:
1. There was no clear scientific problem for this manuscript, which should be proposed clearly and the manuscript should be reorganized accordingly.
2. Why the Fe1-TiO2 was chosen as an example? The catalytic activity was the most highest or some other reasons? It should be provided in the main text.
3. Although a lot of M1-TiO2 single atom catalysts were synthesized, they were not all applied to the plastic recycling.

Besides, the only evidence for the formation of single atoms for other elements except Fe was EDX element mapping. That is far from enough. The Cr, Mn, Ni was too few to be determined as atomic dispersion, while the Cu was too many. Besides, the resolution of the EDX element mapping cannot so precise to see single atoms. That is the universal and scalable of the method to synthesize M1-TiO2 is questionable. The data (Fig. 4e) was not fitted. The mass of metal chloride precursors required for the synthesis of M-TiO2 nanostructures provided in supplementary Table 2 was optimized or not?

4. The evidences for the formation of the Fe single atoms over the TiO2 were not sufficient enough, although the EDS and EELS could give some evidences on local areas. The atomic number of Ti and Fe was very close (their difference is no more than 5), the EXAFS results could not tell their differences. That is, the Ti-O-Fe or Ti-O-Ti could not be clarified (Fig. 1b). The data fitting results in Supplementary Table 1 showed the coordination number of Fe-O of the Fe1-TiO2 was about 4. It was fully coordinated, which indicated that the Fe was not on the surface of TiO2. Besides, the loading of Fe should be confirmed. It is suggested to denote the actual loading determined by ICP with the same unit, e.g., wt% or at%. But the 15wt% and 3.87at% appeared at the same time in the main text, it should be reconsidered to use the same unit.

5. The E0 value of the XANES results of the Fe, Ti etc. should be calculated according to the experimental data to see the valence state of them. The decrease of the intensity of the peaks could not be correlated to the change of the valence state here (Fig 1a).

6. The control experiment on the synthesis of Fe1-TiO2 was performed to say the hydrolysis kinetics could influence the formation of the Fe single atoms. Later for noble metals, the reduction potential could determine the formation of nanoparticles or single atoms. Which one could be the most important one? For the base metals, the reduction potentials were not important?

7. The catalytic performance of the Fe1-TiO2 was evaluated for the photothermal catalytic of PET glycolysis. How about the level of the reaction rate compared with those reported previously? In supplementary Fig. 37, the energy band structures were summarized. What is the purpose? Will these results affect their catalytic performances?

Reviewer #3

(Remarks to the Author)
Liu et al. present a novel method for the scalable synthesis of SACs with high heteroatom loading on TiO2 substrates. They have expanded this method to synthesize a range of metal single atom catalysts, including 15 different unary M1-TiO2 nanostructures, and two types of binary and ternary composites. The authors investigate the influence of various synthesis parameters on the structure and catalytic activity of these materials, particularly for photothermal catalytic polyester recycling using Fe1-TiO2 catalysts. This work is intriguing and contributes significantly to fundamental scientific society such as the single-atom catalysts, plastic recycling, photocatalysis, and solar energy utilization. Consequently, this manuscript is recommended for publication with minor revisions.

(1) The schematic diagram illustrating the synthesis of Fe1/TiO2 nanostructures (Fig. 1b) is overly simplistic and omits essential details. It should be updated to include the mechanism by which Fe single atoms are deposited on TiO2 supports, thereby providing a more detailed visualization of the synthesis process.

(2) The synthesis of Fe1/TiO2 nanostructures occurs under ambient air conditions, which suggests the critical roles of humidity and oxygen. The metal precursor likely adsorbs moisture from the air, aiding the synthesis process. This raises a question about the necessity of solvents like water to enhance moisture adsorption if the precursor's affinity for moisture is insufficient. Moreover, it would be beneficial to explore whether the Fe1/TiO2 nanostructures could be synthesized in oxygen-free conditions.

(3) The authors should clarify how they determined the valence state of elemental Fe in Fe1-TiO2 nanostructures using the absorption edge position in X-ray Absorption Near Edge Structure (XANES) spectroscopy. A detailed explanation of any linear correlation observed would enhance the reader's understanding.

(4) In the production of Fe1-TiO2 catalysts, diethylene glycol (DEG) plays a crucial role. Typically, DEG ligands on the catalyst surface might hinder catalytic activity by blocking active sites or altering surface characteristics. This study takes a novel approach by retaining the DEG ligands, yet the catalyst exhibits excellent performance in photothermal catalysis for polyester up-cycling. The specific reasons for this effectiveness should be thoroughly explained.

(5) Evaluating the performance of the Fe1-TiO2 catalysts in photothermally catalyzed polyester upcycling is crucial. The authors should provide a comparison with other reported works and also describe the stability and morphology of the catalyst post-reaction.

(6) It is advisable to specify the reaction conditions such as temperature, duration, and whether conditions are thermal or photothermal in the figure legends of both the manuscript and supplementary information. Details regarding the extended testing period (20 hours) should also be included.

(7) Detailed purity characterization data for the upcycled polyester product should be provided.

Version 1:

Reviewer comments:

Reviewer #1

(Remarks to the Author)
The authors have addressed the issues raised, however, some of the current formulations as well as the innovations are not convincing before considering this MS to be accepted. The detail suggestions are as following:
1. The authors argue that the single-atom content is a summation of the bulk phase and the surface. There is no different from ordinary doping and has been studied extensively, so the innovativeness of the article needs further elucidation.

2. It is generally accepted that catalytic reactions are surface reactions, therefore accurate quantification of surface-active sites is important and the authors are advised to supplement the surface Fe content.
3. In addition to considering the conversion rate, the by-products of the catalytic process as well as the selectivity should also be considered.
4. In terms of activity, Fe does not show significant advantages over V, Co, Zn, Mo, etc.

Reviewer #2

(Remarks to the Author)
The manuscript improved a lot. Most of the questions were well addressed. It can be accepted.

Reviewer #3

(Remarks to the Author)
In this revision, the authors gave more clarification by citing literature or using additional information on characterization and applications. The quality of this work is obviously improved. I suggest acceptance as it is.

Version 2:

Reviewer comments:

Reviewer #1

(Remarks to the Author)
The author responded in detail to the questions we asked, and the current version is suitable to be accepted.

RESPONSE TO REVIEWERS' COMMENTS

General Comments:

1. All Nature Communications manuscripts must include a "Data Availability" section after the Methods section but before the References.

Response: We have supplied the "Data Availability" with the following statement: The source data generated in this study are provided in the Source Data file. Source data are provided with this paper.

2. To maximise the reproducibility of research data, we strongly encourage you to provide a file containing the raw data underlying the following types of display items:

Response: We have uploaded our original data in the system.

Reviewer 1:

In this manuscript, the M_1-TiO_2 nanostructures with abundant M-O-Ti units are synthesized, and exhibit high efficiency in photochromic photothermal catalysis toward recycling waste polyesters. The authors have done extensive characterization of different single atoms and explained the synthesis process in detail from kinetic and thermodynamic limitation. However, it did not show significant advantages over other synthesis methods. At the same time, the precise sites and the mechanism in catalysis of single atoms are very vague. Taking into account the impact of the journal as well as the completeness and innovation of the current edition, it is not appropriate for the article to be accepted, the detail suggestions are as followed.

Response: Thank you very much for your valuable feedback and detailed suggestions. We appreciate your recognition of our efforts in characterizing different single atoms and explaining the synthesis process in detail. We have carefully considered your comments and have made several revisions to address your concerns:

Significant advantages over other synthesis methods: We have expanded the discussion in the manuscript to more clearly highlight the advantages of our DEG-assisted synthesis strategy over other methods. *Current methodologies are often subject to stringent conditions and are susceptible to oxygen and moisture*. These constraints pose challenges to the scalability of production. Moreover, *most of these approaches exhibit limitations in their universality, allowing for the doping of only a limited set of heteroatoms*. Consequently, the universal and scalable synthesis of M_1-TiO_2, featuring high doping concentrations, continues to present a significant challenge, which primarily arises from the kinetic and thermodynamic limitations. *We present a versatile and scalable synthetic platform for creating M_1-TiO_2 nanostructures with high heteroatom concentrations*. The key to this strategy is the combination of kinetic control involving the passivation of hydrolysis activity of heteroatoms by diethylene glycol and thermodynamic control by introducing short-range order structures to release free energy from lattice mismatch. We believe that this comparative analysis can highlight the impact of this work.

Photochromic single-atom catalysts: Photochromic materials hold significant potential for applications in catalysis. For instance, Prof. Yadong Li and colleagues reported on photochromic Bi_2WO_{6-x}/amorphous BiOCl (*p*-BWO) nanosheets, which show blue coloration upon visible light irradiation and are bleached by atmospheric oxygen. The existence of abundant $W_{(VI)}O_{6-x}$ units serve as the sites for the fast and continuous consumption of photogenerated electrons, thereby effectively facilitating the separation of electron-hole pairs (*Nat. Catal. 2018, 1, 704–710*). Similarly, Prof. Taeghwan Hyeon and collaborators have developed a reversible and synergistic photo-activation process involving individual copper atoms at specific positions (*Nat. Mater. 2019, 18, 620–626*). This process facilitates the manipulation of the valence states of copper atoms in co-catalysts, thereby enabling the reversible regulation of the macroscopic and optoelectronic properties of TiO_2. These results emphasize that photochromic materials, particularly photochromic single-atom catalysts,

possess a variety of crucial applications. However, a universal synthesis approach for structurally controlled photochromic single-atom catalysts is still lacking. *The synthesized M_1-TiO_2 nanostructures exhibit a unique photochromic effect, a feature difficult to achieve with other single atoms.* Therefore, this work represents a significant advance in both material structure and synthesis methods.

Mechanism in catalysis: We have provided a more detailed mechanistic explanation of the catalytic process, *supported by supplemented spectroscopic evidence and computational studies*. This helps clarify how the unique atomic configuration contributes to the observed catalytic efficiency.

Completeness: In light of your comments, we have reorganized the manuscript to ensure a more logical flow of information, from the identification of the scientific problem to the presentation of our innovative solution and its advantages. This includes restructuring sections to improve clarity and coherence, making the narrative more compelling and easier to follow.

We kindly hope you are satisfied with the significant revisions and can reconsider your decision. We believe that the unique aspects of our study, combined with the additional data and improved explanations, make it a valuable addition to the scientific literature. Thank you once again for your constructive feedback.

1. It has been reported that there are simpler ways to synthesize large quantities of single-atom/TiO_2 catalysts, and the current system does not have a high single-atom loading. Therefore, the synthetic method does not show significant advantages.

Response: We thank the reviewer for these constructive comments. Currently, TiO_2-supported single-atom catalysts have emerged as a key research focus. The primary methods for their synthesis include wet-chemical impregnation, high-temperature calcination, high-temperature molten salt. However, these methods typically require operation under stringent conditions, thus challenging to scale up. Additionally, these methods have limited versatility and can incorporate only a restricted range of heteroatoms. To address these issues, we propose an approach that integrates kinetic and thermodynamic controls. Kinetic control is achieved through the use of diethylene glycol (DEG) to passivate the hydrolytic activity of heteroatoms, while thermodynamic control utilizes the introduction of a short-range ordered structure to dissipate free energy arising from lattice mismatches. Implementing this strategy, we have successfully achieved the universal and scalable synthesis of M_1-TiO_2 catalysts. Importantly, the molar ratio of Fe to Ti in our synthesized Fe_1-TiO_2 catalyst is 3.87 at.%, positioning it at the upper level of current capabilities (**Table R1**).

Table R1. Comparison of the molar ratio of M to Ti in reported M_1-TiO_2 catalysts.

Catalyst	Synthesis method	Universality	M/Ti (at.%)
$Ni_{0.034}@TiO_2$[1]	molten salt, 500 °C under N_2 flow	No	1.73
Ni/TiO_2[2]	molten salt, 500 °C under N_2 flow	No	0.56
$CuSA/TiO_2$[3]	calcination, 450 °C	No	1.91
Cr_1/TiO_2[4]	calcination, 400 °C	No	1.27
Cu_1/TiO_2[5]	calcination, 950 °C	No	1.42
Cu_1/TiO_2[6]	calcination, 900 °C	Yes	0.78
Fe_1-TiO_2 (This work)	**220 °C in air**	**Yes**	**3.87**

[1] Zhang, J.; Wang, W.; Chen, X.; Jin, J.; Yan, X.; Huang, J., Single-Atom Ni Supported on TiO_2 for Catalyzing Hydrogen Storage in MgH_2. *J. Am. Chem. Soc.* **2024,** *146* (15), 10432-10442.

[2] Xiao, M.; Zhang, L.; Luo, B.; Lyu, M.; Wang, Z.; Huang, H.; Wang, S.; Du, A.; Wang, L., Molten-Salt-Mediated Synthesis of an Atomic Nickel Co-catalyst on TiO_2 for Improved Photocatalytic H_2 Evolution. *Angew. Chem. Int. Ed.* **2020,** *59* (18), 7230-7234.

[3] Zhang, Y.; Zhao, J.; Wang, H.; Xiao, B.; Zhang, W.; Zhao, X.; Lv, T.; Thangamuthu, M.; Zhang, J.; Guo, Y.; Ma, J.; Lin, L.; Tang, J.; Huang, R.; Liu, Q., Single-Atom Cu Anchored Catalysts for Photocatalytic Renewable H_2 Production With A Quantum Efficiency of 56%. *Nat. Commun.* **2022,** *13* (1), 58.

[4] Shen, Q.; Cao, C.; Huang, R.; Zhu, L.; Zhou, X.; Zhang, Q.; Gu, L.; Song, W., Single Chromium Atoms Supported on Titanium Dioxide Nanoparticles for Synergic Catalytic Methane Conversion under Mild Conditions. *Angew. Chem. Int. Ed.* **2019,** *59* (3), 1216-1219.

[5] Lee, B.; Gong, E.; Kim, M.; Park, S.; Kim, H. R.; Lee, J.; Jung, E.; Lee, C. W.; Bok, J.; Jung, Y.; Kim, Y. S.; Lee, K.; Cho, S.; Jung, J.; Cho, C.; Lebègue, S.; Nam, K. T.; Kim, H.; In, S.; Hyeon, T., Electronic Interaction between Transition Metal Single-Atoms and Anatase TiO_2 Boosts CO_2 Photoreduction with H_2O. *Energy Environ. Sci.* **2022,** *15* (2), 601-609.

[6] Lee, B. h.; Park, S.; Kim, M.; Sinha, A. K.; Lee, S. C.; Jung, E.; Chang, W. J.; Lee, K.; Kim, J. H.; Cho, S.; Kim, H.; Nam, K. T.; Hyeon, T., Reversible and Cooperative Photoactivation of Single-Atom Cu/TiO_2 Photocatalysts. *Nat. Mater.* **2019,** *18* (6), 620-626.

2. The authors only considered the role of Fe in the generation of oxygen defects in the photochromism, whether Fe single atoms can act as catalytic sites was not considered and further theoretical and experimental evidence is needed to demonstrate this.

Response: We sincerely thank the reviewer for pointing out this issue and apologize for the incomplete description of the catalytic sites in our original manuscript. Based on previous literature and theoretical results, the catalysis of polyester glycolysis reactions by metal oxides primarily relies on the oxygen vacancies, as shown in **Fig. R1**. During the reaction process, dissolved PET chains migrate to the catalyst surface, where the coordination-unsaturated metal centers show strong affinity for the oxygen atoms of the ester groups (C=O) in PET chain. This leads to further polarization of the carbonyl

electrons, causing the carbon atoms to carry a partial positive charge (δ^+), which is conducive to the nucleophilic attack by EG molecules.
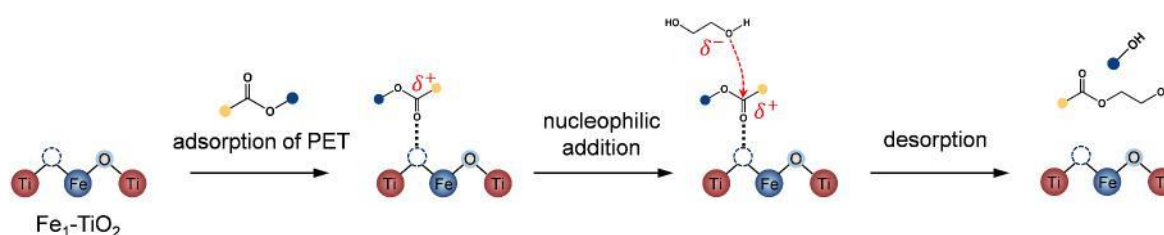

Fig. R1 Schematic illustration of PET glycolysis catalyzed by coordination-unsaturated metal centers.

Experimental evidence:

As highlighted by the reviewer, the catalytic sites for this reaction are likely to be unsaturated coordinated Fe-O_w or Fe-O_w-Ti sites, we first investigated the catalytic performance of commercial Fe_2O_3, FeO, and Fe_3O_4. As shown in **Fig. R2,** the catalytic activities of all samples were poor, which suggests that the contribution of Fe-O_w is excluded. Further studies revealed that the catalytic performance of Fe_1-TiO_2 was significantly higher than that of TiO_2 alone. It was observed that the doped Fe single atoms generated a large number of Fe-O_w-Ti sites on the TiO_2 surface, which accelerated the catalytic reaction. *This enhancement in catalytic activity of Fe_1-TiO_2 can be attributed to the presence of Fe single atoms creating oxygen vacancies*.
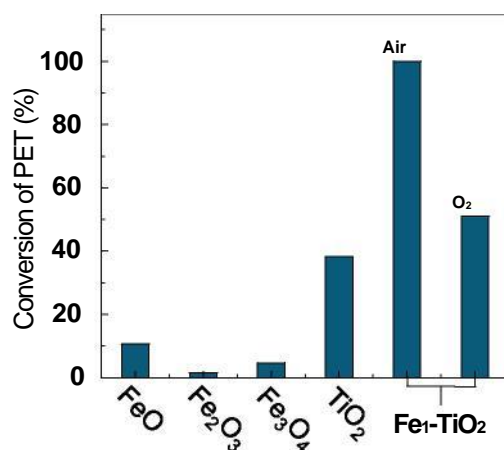

Fig. R2 The catalytic performance of Fe-based catalysts for glycolysis of PET at 190 ^{o}C.

Theoretical Calculations:

To delve into the catalytic mechanism, we embarked on a theoretical investigation of the catalytic mechanism of Fe_1-TiO_2 catalysts in the photothermal-catalyzed PET glycolysis reaction using Density Functional Theory (DFT) calculations. We began by constructing crystal structure models of Fe_1-TiO_2 and TiO_2 catalysts with oxygen vacancies (TiO_2-O_w), as illustrated in **Fig. R3**. Subsequently, we

calculated the charge density differences on the surface of these crystal structures. **Fig. R4a** and **4c** reveal that *in TiO2-Ov catalysts, electrons predominantly cluster around Ti atoms*. In contrast, **Fig. R4b** and **4d** show that *in Fe1-TiO2 catalysts, electrons tend to concentrate near Fe atoms*. This phenomenon can be attributed to the electronegativity difference between Fe and Ti atoms, resulting in a marked increase in electron density on these specific atoms. The charge distribution is visually represented through color-coded electron clouds in these figures. Yellow regions indicate areas of increased charge density, which accumulate around the Fe and Ti atoms following the formation of oxygen vacancies. Conversely, cyan regions signify areas of decreased electron cloud density, typically observed in areas distant from the oxygen vacancies. To further corroborate these observations, we conducted a Bader charge analysis. *This analysis confirmed distinct differences in the charge density distribution of atoms surrounding the oxygen vacancies between the Fe1-TiO2 catalysts and TiO2-Ov* (**Fig. R5**). These differences in electron distribution may play a pivotal role in determining the unique catalytic properties of Fe1-TiO2 catalysts.
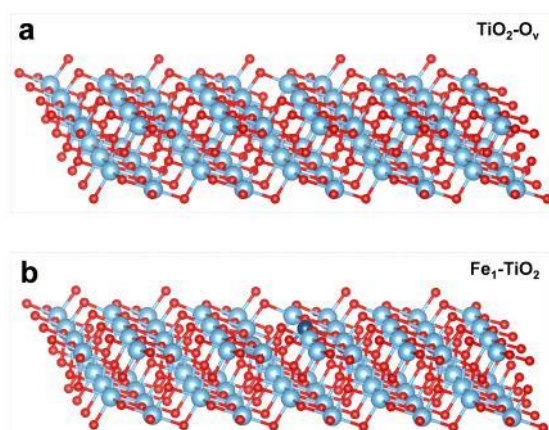

Fig. R3. Schematic illustration of the construction of the (a) TiO2-Ov and (b) Fe1-TiO2 structure model. Atom key: Ti (light blue), Fe (navy) and O (red).
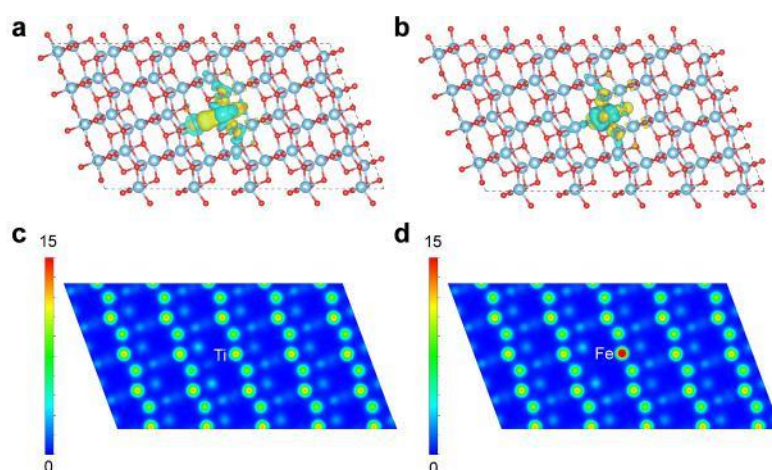

Fig. R4. The charge density distribution of TiO2-Ov and Fe1-TiO2 slabs. 3D charge density for (a) TiO2-Ov and (b) Fe1-TiO2, in which the iso-surfaces are 0.003 e Bohr^{-3}. 2D charge density for (c) TiO2-Ov and (d) Fe1-TiO2.
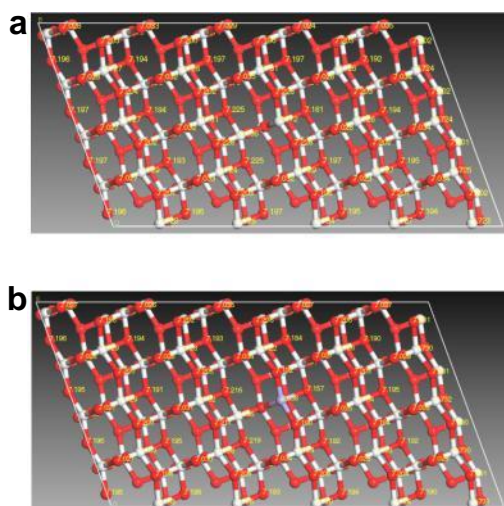
Fig. R5. Calculated Bader charge of (a) TiO_2-O_v and (b) Fe_1-TiO_2 slabs. Atom key: Ti (white), Fe (light purple) and O (red).

The adsorption of PET molecules on the catalyst surface is an important step in PET glycolysis. Therefore, we further investigated the adsorption characteristics of PET on both Fe_1-TiO_2 and TiO_2-O_v catalysts. To simplify the complexity of the calculations, we chose the widely used ethylene glycol dibenzoate (EGD) with a similar structure to PET as a model molecule to calculate the adsorption energies (E_{ads}) (*Nat. Sustain. 2023, 6, 965–973*). As shown in **Fig. R6**, *the E_{ads} value of EGD adsorbed on Fe_1-TiO_2 catalysts (-0.978 eV) is much lower than that adsorbed on TiO_2-O_v catalysts (-0.897 eV), which suggests that Fe-O_v-Ti sites are more preferred for the adsorption of EGDs compared to Ti-O_v-Ti sites*. This preference stems from the modulation of the electronic states of the surrounding atoms by the incorporation of iron singlet atoms. Therefore, it can be inferred that the addition of heteroatoms to TiO_2-O_v alters the interaction between the O_v active site and the EGD molecule. We express our gratitude to the reviewer for your valuable suggestions, which help with improving the clarity of our manuscript.
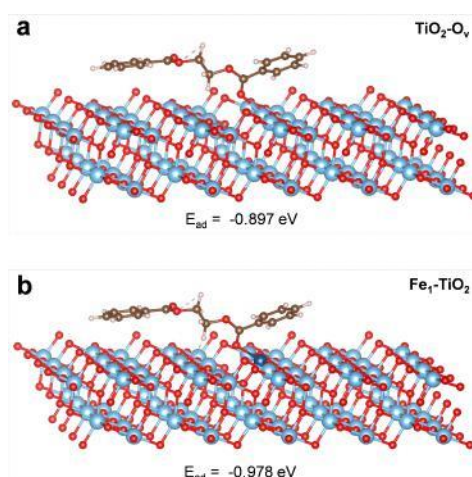

Fig. R6. The adsorbed model and adsorption energy of ethylene glycol dibenzoate (EGD) on (a) TiO_2-O_v and (b) Fe_1-TiO_2 slabs. Atom key: Ti (light blue), Fe (navy), O (red), C (green), H (white).

3. In the Figure 1f, the location marked by the authors is attributed to Ti, whether the material is attributed to oxygen defects or Ti defects?

Response: Thank you for your valuable feedback. We apologize for any confusion caused by the arrow labeling in Figure 1f. We employed AC-STEM (Figure 1f) and geometric phase analysis (Figure 1g) to investigate the crystal defects in TiO_2 and proposed that the lattice distortions may be attributed to oxygen vacancies. We have removed the arrow in the figure and revised the manuscript accordingly.

4. The different valence states Ti achieves cycling during catalysis, and more experimental evidences are needed to prove.

Response: Thank you for your insightful question. In the photothermal polyester upcycling, when the Fe_1-TiO_2 catalysts are exposed to simulated sunlight, they are excited by high-energy UV photons. This excitation leads to the generation of electron-hole pairs. The chemical-bonded DEG ligand effectively captures the holes, thus extending the electron lifetime by preventing rapid carrier recombination (*Angew. Chem. Int. Ed. 2023, 135, e202308930*). Following UV irradiation, there is a significant decrease in the photoluminescence intensity of the Fe_1-TiO_2 catalysts, as illustrated in **Fig. R7a**. This decrease is attributed to the catalyst's black color in its active state, which harbors abundant defect energy levels. These defects facilitate non-radiative carrier relaxation when the excitation light interacts with the catalyst's surface, leading to diminished fluorescence intensity. Further, the absorption spectrum reveals enhanced absorption of visible light, corroborating this observation. Moreover, the longevity of the electron aids in the reduction of Ti^{4+} within the Fe_1-TiO_2 catalysts to Ti^{3+} species, simultaneously generating oxygen vacancies. As demonstrated in **Fig. R7b**, there is a dramatic increase in the count of Ti^{3+} and O_v in the EPR spectra after UV irradiation. This finding suggests that the photogenerated carriers interact primarily with the Fe_1-TiO_2 catalyst itself. The in-situ formed O_v serve as catalytic sites that facilitate the adsorption and activation of C-O and C=O bonds in the PET carbon backbone, ultimately leading to exceptional catalytic performance.
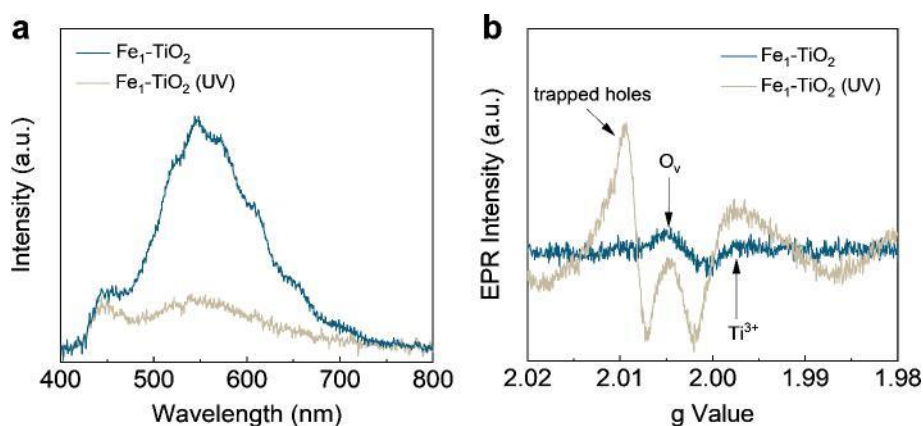

Fig. R7. (a) Photoluminescence and (b) EPR spectra of Fe_1-TiO_2 nanostructures before and after UV exposure for 30 min.

5. In the photocatalytic process, the authors only considered the role of photogenerated electrons in photochromism. Also, electrons can catalyze the generation of oxide species. The authors need further experimental evidence to exclude this effect.

Response: Thank you for your valuable suggestion, which makes our study become integrity and preciseness. In the photochromic processes, the electrons facilitate the reduction of Ti^{4+} to Ti^{3+}, creating oxygen vacancies that serve as catalytic active sites for the glycolysis of PET. However, the excess electrons, in principle, could interact with dissolved O_2 to produce superoxide radicals, potentially influencing the overall reaction.

To further investigate the impact of oxygen on the catalytic glycolysis process, experiments were conducted under both air and nitrogen atmospheres to assess differences in PET conversion and monomer yield. As shown in **Fig. R8a**, the results under a nitrogen are similar to those observed under ambient air conditions. Gas samples extracted during the experiments were analyzed using gas chromatography, which revealed the absence of any carbon-based compounds (**Fig. R8b**). This result preliminarily rules out the contribution of reactive oxygen species. Additionally, we used *p*-benzoquinone (*p*-BQ) as a quenching agent for superoxide radicals to further investigate their potential impact. The addition of *p*-BQ had not affect the catalytic activity or product selectivity (**Fig. R8a**), further ruling out the contribution of reactive oxygen species.

We hypothesize that no reactive oxygen species generated in the system may be due to inadequate UV light intensity within sunlight. Hence, we introduced additional UV light into the solar photothermal catalysis system. By maintaining the same reaction conditions and increasing the UV intensity from 0 to 0.05 W cm^{-2}, the conversion rate of PET increased from 56.0% to 67.9%. The improvement in PET conversion clearly indicates that the UV intensity in the simulated sunlight is insufficient to fully activate the catalytic sites, underscoring no excess photo-generated electrons to generate additional reactive oxygen species.
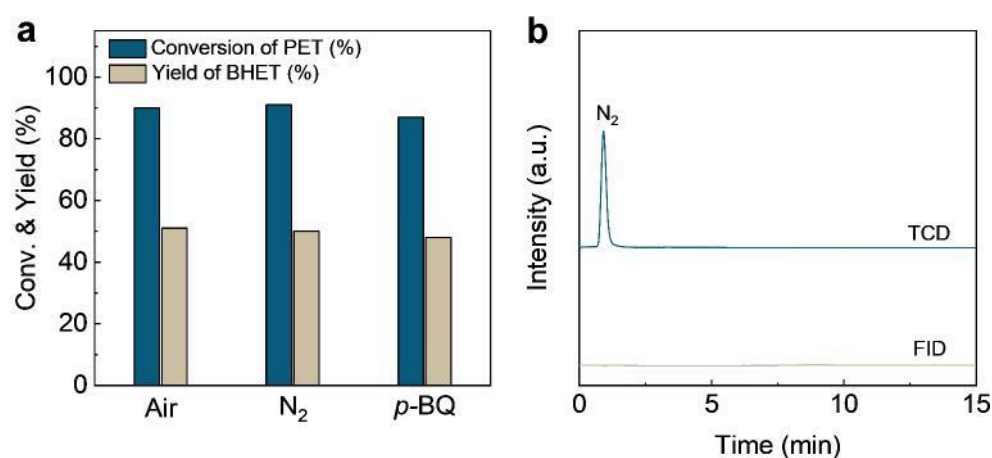

Fig. R8. (a) Effect of reaction atmosphere and quenching agent on catalytic performance of Fe$_1$-TiO$_2$ catalysts. (b) GC of gas-phase after photothermal catalysis in an oxygen atmosphere.

6. In order to highlight the advantages of single atoms in the catalytic process, the authors need to add further experiments related to FeO$_x$ species.

Response: We appreciate your valuable suggestion, which enhances the integrity and precision of our study. To prepare the FeO$_x$/TiO$_2$ catalysts, we increased the Fe/Ti molar ratio to 50% to facilitate the formation of FeO$_x$ supported on TiO$_2$ nanostructures. With the identical catalytic conditions, the PET conversion over the FeO$_x$/TiO$_2$ catalysts (64.4% at 190 °C for 15 min) was lower than that achieved by the Fe$_1$-TiO$_2$ catalysts (100%), highlighting the extraordinary catalytic performance of Fe$_1$-TiO$_2$ catalysts. We thank you again and have incorporated this information into the revised manuscript.

7. The intermediate species in the catalytic process require further experimental and theoretical evidences.

Response: We express our gratitude to the reviewer for the insightful comment. During the reaction process, dissolved PET chains migrate to the catalyst surface, where the coordination-unsaturated metal centers exhibit a strong affinity for the oxygen atoms in the ester groups (C=O) of the PET chain. This interaction further polarizes the carbonyl electrons, causing the carbon atoms to carry a partial positive charge (δ^+), which facilitates the nucleophilic attack by EG molecules.

Experimental evidence:

We first conducted Raman spectroscopy to monitor oxygen vacancy fluctuations after adsorption of BHET, used as a model molecule for PET. As shown in **Fig. R9a**, the oxygen vacancies caused a blue shift in the ν(O-Ti-O) mode of the Fe$_1$-TiO$_2$ catalysts from 143 to 158 cm^{-1} compared to commercial TiO$_2$ (P25). The ν(O-Ti-O) mode redshifted to 153 cm^{-1} when the BHET and Fe$_1$-TiO$_2$ catalysts were mixed and subjected to heat treatment at 110 °C. This result demonstrates that PET is adsorbed on the surface oxygen vacancies of Fe$_1$-TiO$_2$ catalysts.

Additionally, we monitored the activation of BHET over Fe$_1$-TiO$_2$ using FT-IR spectroscopy. As shown in **Fig. R9b**, after mixing BHET with Fe$_1$-TiO$_2$ catalysts and applying heat treatment, the stretching vibrational peaks of the carbonyl group showed a blue shift from 1698 to 1721 cm^{-1}, while the stretching vibrational peaks of the C-O bond exhibited a red shift from 1285 to 1253 cm^{-1}. This indicates that BHET was adsorbed on the oxygen vacancies on the surface of the Fe$_1$-TiO$_2$ catalyst. This adsorption disrupts the conjugated structure between the benzene ring and the carbonyl group in BHET, leading to a bond-weakening effect on the C-O bond, thereby enhancing the electrophilicity of the substrate.
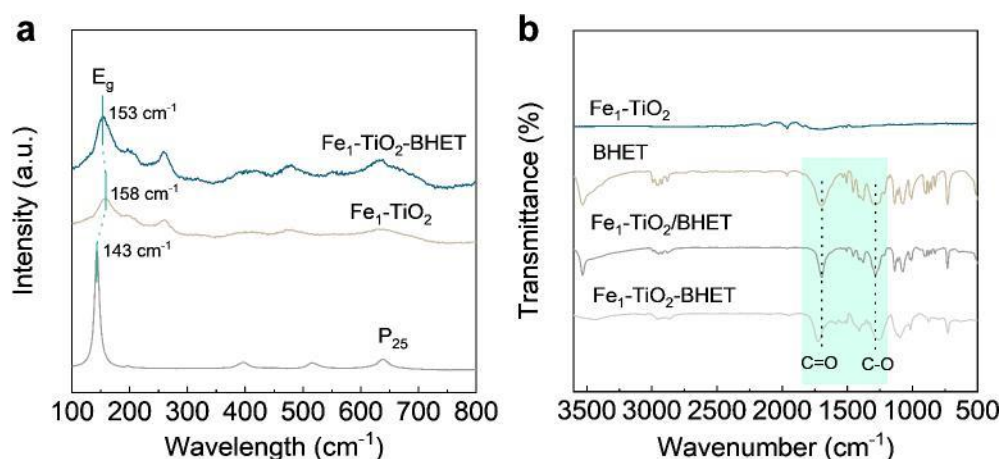
Fig. R9. (a) Raman of Fe$_1$/TiO$_2$ catalysts with BHET adsorption, (b) FT-IR of BHET adsorption on Fe$_1$/TiO$_2$ catalysts.

Theoretical Calculations:

To delve into the catalytic mechanism of Fe$_1$-TiO$_2$ catalysts, we conducted DFT calculations. The structural models (**Fig. R3**), electronic structures (**Fig. R4-R5**), and the adsorption of reactant molecules (**Fig. R6**) were discussed in response to your comments 2.

Then, we conducted Gibbs free energy calculations for each elementary step in the glycolysis of EGD on Fe$_1$/TiO$_2$ and TiO$_2$-O$_w$ catalysts. As illustrated in **Fig. R10**, the glycolysis mechanism is deconstructed into two transition states: initially, an EGD molecule adsorbs on the electron-deficient oxygen vacancy of the catalysts (IS1*), which activate the carbonyl group of EGD. Subsequently, the hydroxyl group of EG undergoes a nucleophilic attack on the carbonyl group to generate another covalent bond (IS2*). Two 2-hydroxyethyl benzoate (2-HB) molecules are formed (IS3*) and then desorbed from the oxygen vacancy (IS4*). As illustrated in **Fig. R10** and **Table R2,** the calculations reveal that in both catalysts, the rate-determining step (RDS) involves the nucleophilic attack of EG to the carbonyl group of the adsorbed EGD. With the Fe$_1$-TiO$_2$ catalysts, the nucleophilic attack of ethylene glycol required only 0.40 eV to surpass the IS2*, whereas the TiO$_2$-O$_w$ catalysts necessitate 0.48 eV. These findings suggest that the adsorption and activation of PET can be effectively enhanced at the Fe-O$_w$-Ti sites, thereby accelerating catalytic performance.
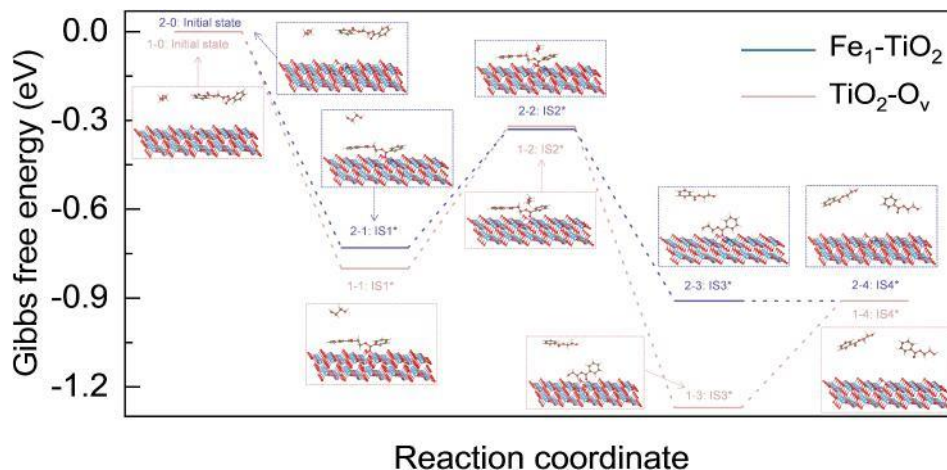
Fig. R10. The intermediate models and calculated Gibbs free energy profiles of photothermal catalytic PET glycolysis on TiO_2-O_v and Fe_1-TiO_2 slabs. Model reaction using Ethylene glycol dibenzoate (EGD) to simulated PET, with Ethylene glycol (EG) as the nucleophile and TiO_2-O_v and Fe_1-TiO_2 as the catalyst, and the products are two molecules of 2-hydroxyethyl benzoate (2-HB). Atom key: Ti (light blue), Fe (navy), O (red), C (green), H (white).

Table R2. Total energy and free energy correction for molecules and reaction intermediates over TiO_2-O_v and Fe_1-TiO_2 slabs for photothermal catalytic PET glycolysis.

Intermediates	E_{DFT} (eV)	E_{ZPE} (eV)	TDS (eV)
Ethylene glycol (EG)	-53.17	2.24	0.94
Ethylene glycol dibenzoate (EGD)	-222.57	7.11	0.94
2-hydroxyethyl benzoate (2-HB)	-137.87	4.67	1.39
TiO_2-O_v	-1855.52	/	/
IS1* on TiO_2-O_v	-2078.99	7.13	0.86
IS2* on TiO_2-O_v	-2132.25	9.40	1.26
IS3* on TiO_2-O_v	-1994.51	4.71	0.67
Fe_1-TiO_2	-1852.24	/	/
IS1* on Fe_1-TiO_2	-2075.79	7.16	0.74
IS2* on Fe_1-TiO_2	-2128.97	9.41	1.28
IS3* on Fe_1-TiO_2	-1991.03	4.72	0.52

8. The catalytic time of 30 min is not sufficient, and further extension is required to further illustrate catalyst stability. And the catalyst needs to be further characterized after the reaction.

Response: Thank you for raising the excellent question. We recognize the importance of evaluating the long-term stability of the catalyst comprehensively. To address this, we carried out seven long-term parallel experiments, aiming to simulate extended reaction periods. Each experiment maintained consistency in terms of the number of reactants (10 g PET and 20 g EG), catalyst dosage (2 mg Fe-TiO$_2$), light intensity (0.68 W·cm^{-2}), and reaction temperature (170 °C). The sole parameter that varied was the reaction time, set at 10 hours, 12.5 hours, 15 hours, 17.5 hours, 20 hours, 22.5 hours and 25 hours, respectively. Notably, to accommodate longer reaction times, we reduced the catalyst dosage to 2 mg while keeping other conditions consistent with the typical reaction conditions. In **Fig. R11a**, we present the relationship between the conversion rate and reaction time for the seven parallel experiments. The gradual increase in the conversion rate of PET with increasing reaction time is evident. Following the literature, PET glycolysis is typically a first-order reaction. The linear fit of the data from **Fig. R11a** demonstrates a perfect linear relationship (**Fig. R11b**), indicating that the catalyst's activity remains robust even under prolonged illumination. This observation assures us of the catalyst's excellent stability over extended reaction times.
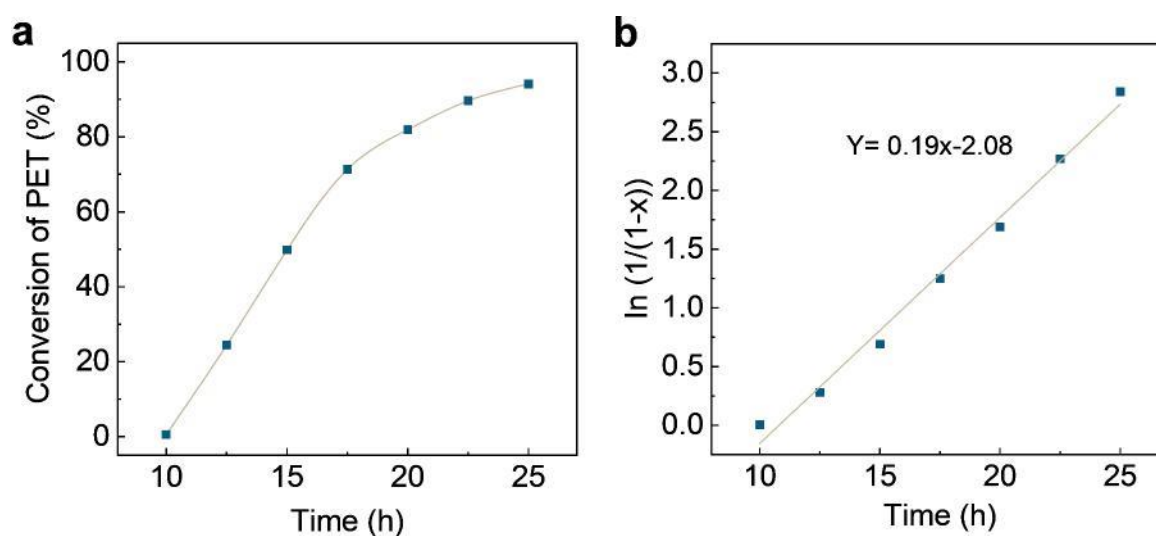

Figure R11. (a) The conversion of PET at different times and (b) The linear fit to the PET conversion versus reaction time of Fe$_1$-TiO$_2$ nanostructures.

The structure of the spent Fe$_1$-TiO$_2$ catalysts were further characterized. As depicted in **Fig. R12**, no distinct Fe-related species in the XRD patterns, coupled with the uniform distribution of Fe elements in EDS mapping, both confirmed no aggregation of Fe species. Moreover, Fourier-transform EXAFS analysis of the spent Fe$_1$-TiO$_2$ catalysts indicates that the Fe atoms were exclusively coordinated with oxygen atoms, evidenced by a prominent peak of Fe-O scattering at approximately 1.57 Å. Notably, no Fe-Fe peak was detected at approximately 2.18 Å, confirming that the Fe single atoms were maintained within the spent Fe$_1$-TiO$_2$ catalysts (**Fig. R13**). These findings collectively

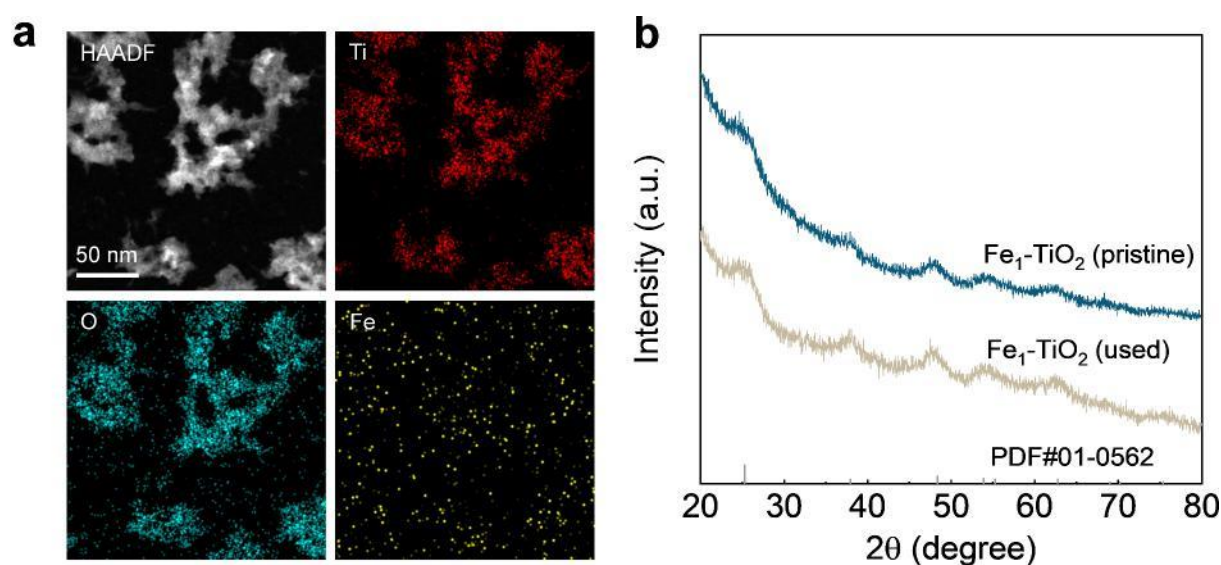affirm the exceptional stability of the Fe₁-TiO₂ nanostructures following the polyester upcycling reaction.

Fig. R12. (a) Elemental mappings and (b) XRD patterns of Fe₁-TiO₂ nanostructures after 25 h reaction.
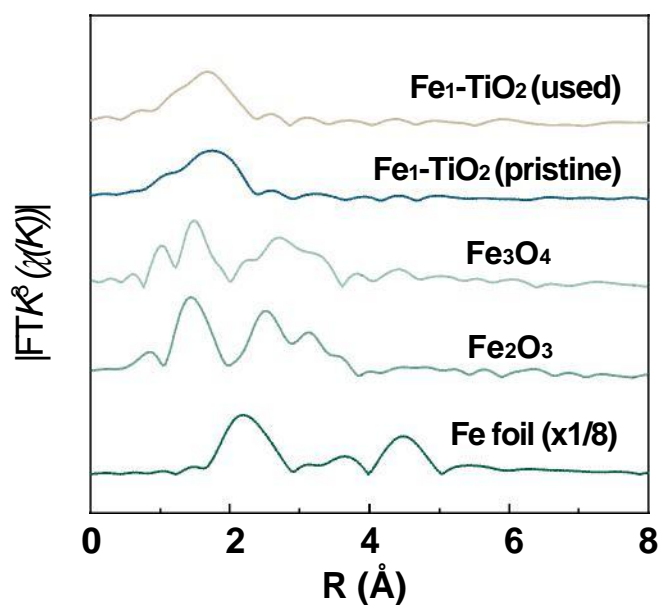
Fig. R13. Normalized FT-EXAFS spectra of pristine and used Fe₁-TiO₂.

9. The authors need to add a comparison of activity relative to other reported catalysts.

Response: Thank you very much for your constructive question. **Table R3** lists the performance of previously reported catalytic systems for the glycolysis of PET. Notably, under the similar reaction conditions, the Fe₁-TiO₂ catalyst provided comparable or even higher space-time yields (STY).

Table R3. Comparison of catalytic performance of reported catalysts for the glycolysis of PET.

Catalyst	Catalyst amount (g)	PET (g)	Time (h)	BHET Yield (%)	STY@190°C ($g_{BHET} \cdot g_{Cat.}^{-1} \cdot h^{-1}$)
Zn(Ac)$_2$	0.29	30	1	68.0	93.06
ZnFe$_2$O$_4$	0.20	5	6	79.5	4.38
OPA@Fe$_3$O$_4$	0.048	0.48	1.5	91.0	8.03
Fe$_3$O$_4$@SiO$_2$@(mim)[FeCl$_4$]	0.015	0.1	24	50.0	0.18
Zinc plates	2	5	5	77.7	0.51
Zn-BDC	0.06	6	3	87.3	38.49
SiO$_2$-Fe$_2$O$_3$-NH$_2$SB NP	0.1	1	3	73.0	3.22
[Ch][OAc]	0.25	5	3	83.8	7.39
t-BuP$_2$	0.25	0.5	1.5	92.7	1.64
4Ti/SBA-15	0.05	0.4	3/4	87.2	12.30
Fe$_3$O$_4$-CP NPs	0.01	1	2	56.9	37.64
ZnO-Fe$_3$O$_4$ HMNAs	0.5	1.5	0.5	92.3	7.33
Zn(OAc)$_2$	0.5	1.5	1/12	83.0	38.75
MeONa	0.28	1	2	75.0	1.77
[HDBU]Im	0.25	5	2/3	78.9	31.16
Cyanamide	0.1	2	2.5	95.2	10.08
MAF-6	0.05	5	4	78.3	25.89
ZnCl$_2$	1	5	2	81.1	2.68
CoCl$_2$	1	5	2	72.7	2.40
Mo/ZnO	0.01	1	1	92.3	122.11
GCNC	0.05	2	0.5	75.0	79.38
[Bmim]HCO$_3$	0.1	2	2	71.2	9.42
1,3-DMU/Zn(OAc)$_2$	0.25	5	1/3	82.0	65.75
rGO/[TESPMI]$_2$CoCl$_4$	0.15	1	3	87.3	2.57
NaHCO$_3$	0.25	5	3	48.0	4.23
Fe$_1$-TiO$_2$ (This work)	0.02	0.5	1/4	76.2	**100.81**

Reviewer 2:

The research on the universal and scalable synthesis of single-atom catalysts and their application for plastic recycling are interesting. In this manuscript, the synthesis of supported M_1-TiO_2 single atom catalysts was claimed to be succeeded for about 20 different elements. The Fe_1-TiO_2 single atom catalyst was chosen as an example characterized by various techniques and applied to the photothermal catalysis of plastics including films, PET and so on. A lot of work had been done, but reorganization was needed. It can be resubmitted if the following questions could be carefully considered.

Response: Thank you for taking the time to review our manuscript. We appreciate your interest in the universal and scalable synthesis of single-atom catalysts and your recognition of the importance of addressing the issue of plastic pollution. We have carefully considered your comments and have incorporated revisions into the manuscript. We believe that the revised version now better presents the key aspects of our research. Thank you for recommending our work for resubmission.

1. There was no clear scientific problem for this manuscript, which should be proposed clearly and the manuscript should be reorganized accordingly.

Response: Thank you very much for pointing out this issue. We apologize for the unclear description in the manuscript. The research ideas of this work are as follows:

Motivation and Key Challenges: The crux of functional nanomaterials lies in the precise synthetic control of nanocrystal compositions at the atomic scale. Semiconducting metal oxide nanomaterials exhibit significant promise in diverse fields such as optoelectronics, batteries, heterogeneous catalysis, and photocatalysis. To maximize the benefits of these applications, a burgeoning avenue involves the atomic doping of these materials with foreign elements. This process not only tunes lattice oxygen activity but also enhances the substrate's electronic structure, surface acidity/basicity, and photon absorption. *However, the pursuit of a universal and scalable synthesis approach with high heteroatom concentrations poses a formidable challenge, primarily due to pronounced structural disparities between M_{hetero}-O and M_{sub}-O units*. Our research, centered on TiO_2 as the exemplified substrate, introduces a diethylene glycol-assisted synthetic platform meticulously designed for the controlled library preparation of various types of M_1-TiO_2 single-atom catalysts with high heteroatom concentrations. We firmly believe that our work holds substantial value for diverse topics thanks to several key discoveries:

Mechanism Innovation: The introduction of DEG affords precise kinetic control by passivating the hydrolytic activity of heteroatom and achieves thermodynamic control by introducing short-range order structures to dissipate the free energy associated with heteroatom incorporation.

Strategy effectiveness: We reveal that unary, binary, or ternary transition metal dopants in a broad range (M = V, Cr, Mn, Fe, Co, Ni, Cu, Zn, Ga, Zr, Nb, Mo, Sn, Ta, W, etc.) can be homogeneously and atomically incorporated into TiO_2 substrate. The heteroatom concentrations can be as high as 5%

(M_{hetero}/Ti atomic ratio).

Catalysis Enhancement: The introduction of heteroatoms in the TiO_2 substrate increases the number of active sites and simultaneously enhances the photochromic photothermal conversion capability. Consequently, the single-atom M_1-TiO_2 catalysts facilitate the photothermal conversion of various real-word waste plastics into value-added monomers.

In short, *this manuscript addresses the key scientific issue of the controllable preparation of photochromic single-atom catalysts, proposes corresponding strategies, and applies the prepared catalysts to the field of plastic recycling*. Based on the above logic and ideas, we have revised and reorganized the text accordingly. Thank you again for your constructive suggestions.

2. Why the Fe_1-TiO_2 was chosen as an example? The catalytic activity was the most highest or some other reasons? It should be provided in the main text.

Response: We appreciate the reviewer's thoughtful comments. The selection of the Fe_1-TiO_2 catalyst as an example was primarily based on two reasons. *Firstly, Fe_1-TiO_2 catalysts have been widely applied in various significant research areas such as photocatalysis, environmental treatment, energy conversion, and organic synthesis. Achieving controllable preparation of this catalyst is expected to have direct applications in these fields. Secondly, during the catalyst screening process, we observed that the Fe_1-TiO_2 catalyst also exhibited top-tier activity in the photothermal catalytic glycolysis of PET (Fig. R14)*. Based on these two reasons, we chose Fe_1-TiO_2 as the research model. We apologize for not making this clear in the manuscript due to our oversight. In the revised version, we have added a discussion on this aspect.
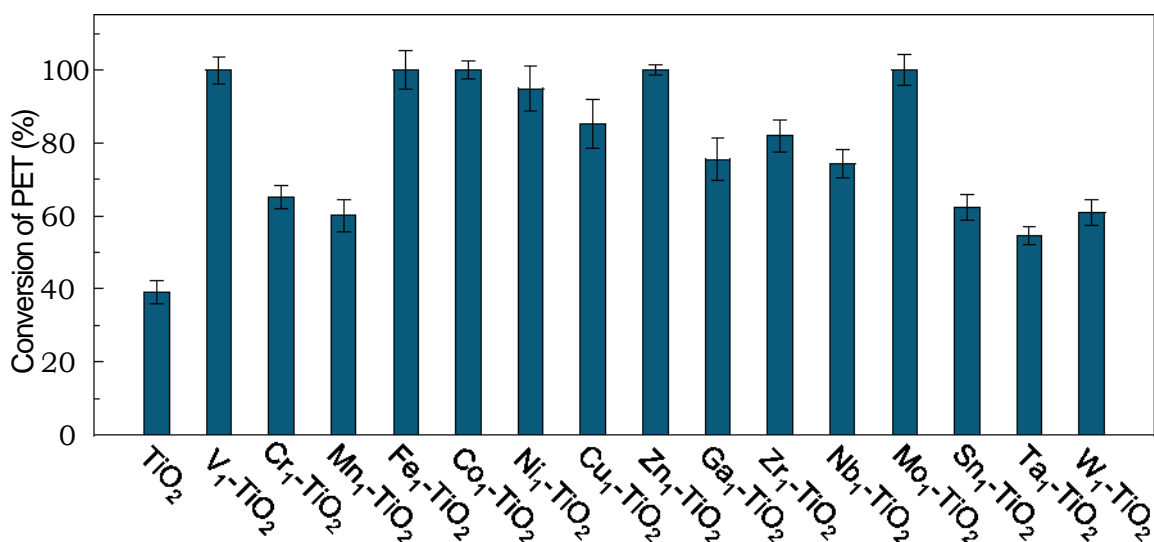

Fig. R14. The catalytic performance of M_1-TiO_2 nanostructures for photothermal catalytic PET plastic upcycling.

3. Although a lot of M_1-TiO_2 single atom catalysts were synthesized, they were not all applied to the plastic recycling. Besides, the only evidence for the formation of single atoms for other elements except Fe was EDX element mapping. That is far from enough. The Cr, Mn, Ni was too few to be determined as atomic dispersion, while the Cu was too many. Besides, the resolution of the EDX element mapping cannot so precise to see single atoms. That is the universal and scalable of the method to synthesize M_1-TiO_2 is questionable. The data (Fig. 4e) was not fitted. The mass of metal chloride precursors required for the synthesis of M_1-TiO_2 nanostructures provided in supplementary Table 2 was optimized or not?

Response: We thank the reviewer for these constructive comments, which will significantly enhance the quality of our work. Firstly, we have supplemented the catalytic performance data for all single-atom catalysts. As shown in **Fig. R14**, all the single-atom catalysts exhibited catalytic activity superior to that of TiO_2, which underscores the significant role of this unique structure in enhancing catalytic performance.

Regarding the structural characterization of single-atom catalysts, we have made the following supplementary. The ideal methods for characterizing single-atom materials are synchrotron spectroscopy and aberration-corrected high-angle annular dark-field scanning transmission electron microscopy (AC-HAADF-STEM). Due to constraints on synchrotron testing time, we were unable to characterize all M_1-TiO_2 catalysts. *Nevertheless, we made every effort to measure as many single-atom catalysts as possible. We would like to emphasize that the characterized samples chosen are those where single-atom formation is more challenging.* For example*, despite the significant difference in atomic radii between Mo and Ti, which could theoretically lead to large lattice mismatch and potential agglomeration to form MoO_x, the Mo K-edge EXAFS results confirm the atomically dispersed states of Mo in Fe_1Mo_1-TiO_2.* Furthermore, *the EXAFS spectra show that even in structurally complex ternary-doped systems, single-atom structures ($Fe_1Co_1Cu_1$-TiO_2) can be obtained*. These spectroscopic results indicate the universality of our synthesis method. We hope you can understand our characterization efforts.

To further enhance the credibility of our product characterization, we supplemented with AC-HAADF-STEM characterization. As is well known, AC-HAADF-STEM is the most intuitive method for confirming the presence of isolated metal single atoms, relying on Rutherford scattering. This technique is highly sensitive to variations in the atomic number of atoms in the sample (Z-contrast images), where the image intensity of a specific atom is directly proportional to the square of the elemental atomic number (Z^2). In essence, the higher the Z value of an element, the brighter its image appears. In this work, direct observation by AC-HAADF-STEM is challenging due to the majority of heteroatoms' atomic numbers being close to that of Ti. Given the substantial difference in atomic numbers between Mo (Z = 42) and Ti (Z = 22), Fe_1Mo_1-TiO_2 nanostructures were selected as a representative sample for AC-HAADF-STEM characterization, where Mo in Mo_1-TiO_2 exists in an atomically dispersed state (marked with bright red circles, **Fig. R15**).

Additionally, the use of EDS was intended only to demonstrate the uniform dispersion of elements and not to confirm the single-atom structure. We apologize for any misunderstanding this may have caused. The strong signal from Cu elements may be attributed to the use of a Cu grid during the TEM characterization. We hope that the explanations and additional experiments provided will enhance the credit of this work. We have also supplemented the EXAFS fitting results of Fig. 4e in the **Table R4** and revised supporting information. In addition, the mass of the metal chloride precursor listed in Supplementary Table 2 are intended to maintain the M/Ti feed molar ratio at 5 at.%, and we sincerely apologize for not labeling it initially. The correction has been made in the revised manuscript.
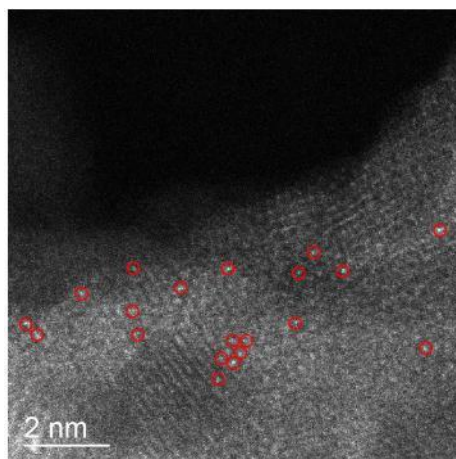

Fig. R15. AC-HAADF-STEM image of Fe_1Mo_1-TiO_2 nanostructures.

Table R4. The EXAFS fitting results of Fig. 4e in R space.

Sample	Scattering path	CN	R (Å)	σ^2 ($10^{-3} \cdot Å^2$)	ΔE_0 (eV)
Fe foil	Fe-Fe$_1$	8	2.46 ± 0.02	5.83 ± 2.03	5.01 ± 2.74
	Fe-Fe$_2$	6	2.84 ± 0.01	5.30 ± 2.75	5.01 ± 2.74
Fe$_3$O$_4$	Fe-O$_1$	4	2.04 ± 0.02	7.96 ± 3.27	8.89 ± 1.72
	Fe-O$_2$	2	2.35 ± 0.04	8.04 ± 4.58	8.89 ± 1.72
	Fe-Fe$_1$	6	3.08 ± 0.02	14.8 ± 2.85	8.89 ± 1.72
	Fe-Fe$_2$	4	3.55 ± 0.02	9.57 ± 3.27	8.89 ± 1.72
CuO	Cu-O	4	1.96 ± 0.02	3.75 ± 3.60	8.36 ± 2.14
	Cu-Cu	4	2.95 ± 0.03	9.31 ± 3.97	8.36 ± 2.14
Co$_3$O$_4$	Co-O$_1$	2	1.93 ± 0.06	4.00	2.95 ± 1.58
	Co-O$_2$	4	1.90 ± 0.05	9.24	2.95 ± 1.58
	Co-Co$_1$	4	2.87 ± 0.01	3.00	2.95 ± 1.58
	Co-Co$_2$	2	3.22 ± 0.08	4.09	2.95 ± 1.58
	Co-Co$_3$	2	3.34 ± 0.02	3.67 ± 1.25	2.95 ± 1.58
	Co-Co$_4$	4	3.44 ± 0.04	3.00	2.95 ± 1.58
MoO$_3$	Mo-O$_1$	1	1.74 ± 0.03	3.00	2.95 ± 1.58
	Mo-O$_2$	1	1.68 ± 0.02	3.00	2.95 ± 1.58

		CN	R	σ^2	ΔE_0
	Mo-O$_3$	2	1.96 ± 0.01	3.00	2.95 ± 1.58
	Mo-O$_4$	1	2.20 ± 0.02	3.00	2.95 ± 1.58
	Mo-O$_5$	1	2.33 ± 0.02	3.00	2.95 ± 1.58
	Mo-Mo$_1$	2	3.41 ± 0.02	3.47 ± 1.65	2.95 ± 1.58
	Mo-O$_6$	4	3.38 ± 0.05	10.1 ± 6.91	2.95 ± 1.58
	Mo-Mo$_2$	2	3.80 ± 0.01	6.57 ± 6.41	2.95 ± 1.58
	Mo-O$_7$	2	3.89 ± 0.10	3.00	2.95 ± 1.58
	Mo-Mo$_3$	2	4.03 ± 0.03	3.00	2.95 ± 1.58
Mo foil	Mo-Mo$_1$	8	2.72 ± 0.01	3.58 ± 1.64	3.37 ± 1.92
	Mo-Mo$_2$	6	3.13 ± 0.01	3.33 ± 2.19	3.37 ± 1.92
NiO	Ni-O	6	2.09 ± 0.04	16.1 ± 7.86	0.40 ± 2.88
	Ni-Ni	6	2.96 ± 0.02	3.58 ± 2.29	0.40 ± 2.88
Fe in Fe$_1$Co$_1$Cu$_1$-TiO$_2$	Fe-O	3.29 ± 1.53	2.15 ± 0.05	6.12 ± 9.60	8.91 ± 4.22
Co in Fe$_1$Co$_1$Cu$_1$-TiO$_2$	Co-O	3.38 ± 1.06	2.12 ± 0.04	3.55 ± 5.67	18.5 ± 2.9
Cu in Fe$_1$Co$_1$Cu$_1$-TiO$_2$	Cu-O	3.50 ± 1.06	2.01 ± 0.08	6.00	25.2 ± 14.9
Fe in Fe$_1$Mo$_1$-TiO$_2$	Fe-O	3.69 ± 0.72	2.03 ± 0.03	6.10 ± 3.74	1.21 ± 2.15
	Mo-O$_1$	2.32 ± 0.41	1.72 ± 0.05	4.78	0 ± 10.65
Mo in Fe$_1$Mo$_1$-TiO$_2$	Mo-O$_2$	0.69 ± 0.83	2.06 ± 0.14	6.59	0 ± 10.65
	Mo-O$_3$	1.06 ± 1.53	2.41 ± 0.09	6.00	0 ± 10.65
Ni$_1$-TiO$_2$	Ni-O	6.35 ± 1.20	2.12 ± 0.02	12.2 ± 4.2	4.34 ± 1.72
Fe$_1$-TiO$_2$	Fe-O	3.33 ± 0.40	2.07 ± 0.03	4.00	8.74 ± 2.46

CN: coordination number; R: interatomic distance; σ^2: Debye-Waller factor; ΔE_0: energy deviation; S_0^2: Amplitude reduction factor, 0.90.

4. The evidence for the formation of the Fe single atoms over the TiO$_2$ were not sufficient enough. The atomic number of Ti and Fe was very close (their difference is no more than 5), the EXAFS results could not tell their differences. That is, the Ti-O-Fe or Ti-O-Ti could not be clarified (Fig. 1b). The data fitting results in Supplementary Table 1 showed the coordination number of Fe-O of the Fe$_1$-TiO$_2$ was about 4. It was fully coordinated, which indicated that the Fe was not on the surface of TiO$_2$. Besides, the loading of Fe should be confirmed. It is suggested to denote the actual loading determined by ICP with the same unit, e.g., wt% or at%. But the 15wt% and 3.87at% appeared at the same time in the main text, it should be reconsidered to use the same unit.

Response: We appreciate the reviewer's thoughtful comment and apologize for any confusion caused. The close proximity of the atomic numbers of Ti and Fe poses a significant challenge in distinguishing them. Despite efforts by some studies to address this issue, this difficulty often leads to controversial interpretations in the literature (*Angew. Chem. Int. Ed. 2020, 59, 15855-15859; Nat. Mater. 2019, 18, 620-626; Nat. Commun. 2023, 14, 1117*). Therefore, we have removed the distinction between Fe-O-Ti and Ti-O-Ti in the revised manuscript. Additionally, in our EXAFS spectra, we observed a strong

Fe-O scattering path but no obvious Fe-O-Fe scattering path, collectively confirming that the prepared structure is a single-atom structure. We apologize for the confusion regarding the coordination number. Based on your suggestion, we have carefully fitted the EXAFS data of all samples (Table R4). Our results indicate that the heteroatoms are coordinated unsaturated, suggesting that heteroatoms are present both on the surface and inside. Thank you again for your in-depth analysis of this issue. In addition, as per your suggestion, we have also normalized the actual loadings determined by ICP to atomic percentages (at.%).

5. The E_0 value of the XANES results of the Fe, Ti etc. should be calculated according to the experimental data to see the valence state of them. The decrease of the intensity of the peaks could not be correlated to the change of the valence state here (Fig 2a).

Response: We thank the you for the constructive suggestion. Accordingly, we have calculated the E_0 value of the XANES results for the Fe, Ti et. in all samples. We have also supplemented the E_0 value in the **Table R5** and revised supporting information. By plotting the energy threshold position, which increases with the oxidation state (**Fig. R16**), the precise oxidation state of Fe in the catalysts were calculated. Fe_2O_3 exhibits the highest oxidation state, close to +3, followed by Fe_1-TiO_2, with a valence state of +2.7.

Table R5. The E_0 value of the XANES results for all samples.

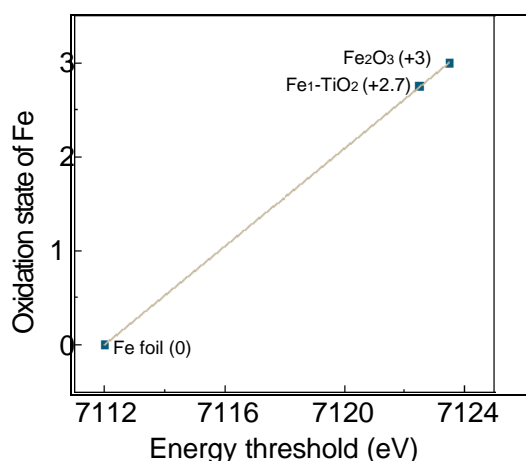| Figure	Sample	Threshold engergy (E_0, eV)
2a	TiO_2	4983.1
	Fe_1-TiO_2	4980.4
2b	Fe foil	7112.0
	Fe_1-TiO_2	7122.5
	Fe_3O_4	7121.7
	Fe_2O_3	7123.5
4e	Cu in $Fe_1Co_1Cu_1$-TiO_2	8985.6
	CuO	8987.2
	Co in $Fe_1Co_1Cu_1$-TiO_2	7718.9
	Co_3O_4	7719.1
	Fe in $Fe_1Co_1Cu_1$-TiO_2	7121.4
	Fe in Fe_1Mo_1-TiO_2	7124.5
	Mo in Fe_1Mo_1-TiO_2	20016.1
	Mo foil	20000.0
	MoO_3	20016.1
	Ni-TiO_2	8345.8
	NiO	8345.2

Fig. R16. Plot of oxidation states of Fe in Fe_1-TiO_2 and references as determined from the edge positions in the Fe K-edge XANES spectra.

6. The control experiment on the synthesis of Fe_1-TiO_2 was performed to say the hydrolysis kinetics could influence the formation of the Fe single atoms. Later for noble metals, the reduction potential could determine the formation of nanoparticles or single atoms. Which one could be the most important one?

Response: Thank you very much for your question. We sincerely apologize for any misunderstanding caused by our phrasing in the original manuscript. In this work, it is essential that the metal precursors possess properties that make them difficult to reduce. This is because metal precursors that are easily reducible can be rapidly reduced by diethylene glycol (DEG) to form metal nanoparticles, which do not embed into the TiO_2 lattice to form single-atom structures but rather metal nanoparticles-loaded TiO_2 structures. *Therefore, the difficulty in reducing the precursor is a necessary condition for the formation of single-atom structures. Only when this condition is met can we discuss the impact of hydrolysis kinetics on the structure of the product.* Thank you once again for your question; we have clarified this point in the revised manuscript.

7. The catalytic performance of the Fe_1-TiO_2 was evaluated for the photothermal catalytic of PET glycolysis. How about the level of the reaction rate compared with those reported previously? In supplementary Fig. 37, the energy band structures were summarized. What is the purpose? Will these results affect their catalytic performances?

Response: Thank you very much for your constructive question. **Table R3** lists the performance of previously reported catalytic systems for the glycolysis of PET. Under similar reaction conditions, the Fe_1-TiO_2 catalyst provided comparable or even higher space-time yields (STY). In addition, Supplementary Fig. 37 is included to demonstrate that our synthesis method can prepare photochromic single-atom catalysts with tunable band structures. Although its direct relevance to the current study may be limited, our goal is to provide a reference library to support other fields, such as photocatalysis,

with relevant theoretical foundations and data.

Table R3. Comparison of catalytic performance of reported catalysts for the glycolysis of PET.

Catalyst	Catalyst amount (g)	PET (g)	Time (h)	BHET Yield (%)	STY @ 190 °C ($g_{BHET} \cdot g_{Cat.}^{-1} \cdot h^{-1}$)
$Zn(Ac)_2$	0.29	30	1	68.0	93.06
$ZnFe_2O_4$	0.20	5	6	79.5	4.38
$OPA@Fe_3O_4$	0.048	0.48	1.5	91.0	8.03
$Fe_3O_4@SiO_2@(mim)[FeCl_4]$	0.015	0.1	24	50.0	0.18
Zinc plates	2	5	5	77.7	0.51
Zn-BDC	0.06	6	3	87.3	38.49
SiO_2-Fe_2O_3-NH_2SB NP	0.1	1	3	73.0	3.22
[Ch][OAc]	0.25	5	3	83.8	7.39
t-BuP_2	0.25	0.5	1.5	92.7	1.64
4Ti/SBA-15	0.05	0.4	3/4	87.2	12.30
Fe_3O_4-CP NPs	0.01	1	2	56.9	37.64
ZnO-Fe_3O_4 HMNAs	0.5	1.5	0.5	92.3	7.33
$Zn(OAc)_2$	0.5	1.5	1/12	83.0	38.75
MeONa	0.28	1	2	75.0	1.77
[HDBU]Im	0.25	5	2/3	78.9	31.16
Cyanamide	0.1	2	2.5	95.2	10.08
MAF-6	0.05	5	4	78.3	25.89
$ZnCl_2$	1	5	2	81.1	2.68
$CoCl_2$	1	5	2	72.7	2.40
Mo/ZnO	0.01	1	1	92.3	122.11
GCNC	0.05	2	0.5	75.0	79.38
$[Bmim]HCO_3$	0.1	2	2	71.2	9.42
1,3-DMU/$Zn(OAc)_2$	0.25	5	1/3	82.0	65.75
$rGO/[TESPMI]_2CoCl_4$	0.15	1	3	87.3	2.57
$NaHCO_3$	0.25	5	3	48.0	4.23
Fe_1-TiO_2 (This work)	0.02	0.5	1/4	76.2	**100.81**

Reviewer #3:

Liu et al. present a novel method for the scalable synthesis of SACs with high heteroatom loading on TiO$_2$ substrates. They have expanded this method to synthesize a range of metal single atom catalysts, including 15 different unary M$_1$-TiO$_2$ nanostructures, and two types of binary and ternary composites. The authors investigate the influence of various synthesis parameters on the structure and catalytic activity of these materials, particularly for photothermal catalytic polyester recycling using Fe$_1$-TiO$_2$ catalysts. This work is intriguing and contributes significantly to fundamental scientific society such as the single-atom catalysts, plastic recycling, photocatalysis, and solar energy utilization. Consequently, this manuscript is recommended for publication with minor revisions.

Response: We appreciate your positive evaluation of our work and recognition of the novelty of our proposed a novel method for the scalable synthesis of SACs with high heteroatom loading on TiO$_2$ substrates. We agree that the concept is intriguing and has the potential for significant contributions to the field of photothermal catalysis. We have carefully considered your comments and have incorporated revisions into the manuscript. We believe that the revised version now better presents the key aspects of our research. Thank you for recommending our work for publication.

1. The schematic diagram illustrating the synthesis of Fe$_1$/TiO$_2$ nanostructures (Fig. 1b) is overly simplistic and omits essential details. It should be updated to include the mechanism by which Fe single atoms are deposited on TiO$_2$ supports, thereby providing a more detailed visualization of the synthesis process.

Response: Thank you for the valuable suggestion. Your feedback is invaluable in enhancing the quality of the synthetic schematic diagram. Following your suggestion, we have created a new synthetic diagram illustrating the entire experimental process. The reactants, reaction conditions, precursors, and the reaction process are now presented more clearly. The new synthetic diagram as shown in **Fig. R17**.
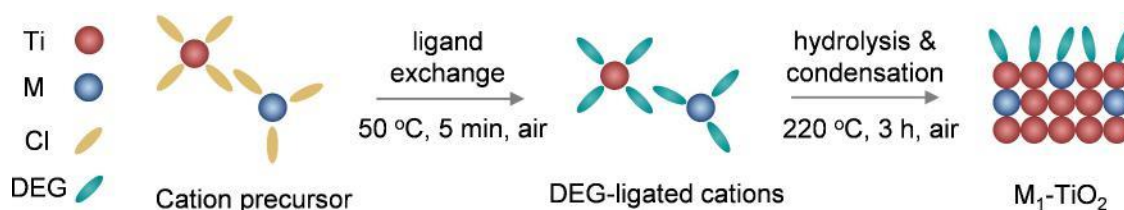

Fig. R17. Schematics of M$_1$-TiO$_2$ nanostructures synthesis via DEG-assisted method.

2. The synthesis of Fe$_1$/TiO$_2$ nanostructures occurs under ambient air conditions, which suggests the critical roles of humidity and oxygen. The metal precursor likely adsorbs moisture from the air, aiding the synthesis process. This raises a question about the necessity of solvents like water to enhance moisture adsorption if the precursor's affinity for moisture is insufficient. Moreover, it would be beneficial to explore whether the Fe$_1$/TiO$_2$ nanostructures could be synthesized in oxygen-free

conditions.

Response: Thank you for your insightful comments. Waster is essential for the synthesis of Fe_1-TiO_2 nanostructures as it influences the hydrolysis rate of heteroatoms and Ti precursors. An extra 0.4 mL of H_2O was added in this work. However, it was found that oxygen had no significant effect on the synthesis of Fe_1-TiO_2 nanostructures. As shown in **Fig. R18**, the morphology and crystal structure of the samples synthesized in nitrogen environment are similar to those of Fe_1-TiO_2 nanostructures synthesized in air. This similarity is due to the polymerization and hydrolysis of Fe-DEG and Ti-DEG complexes does not depend on the involvement of oxygen in the reaction.
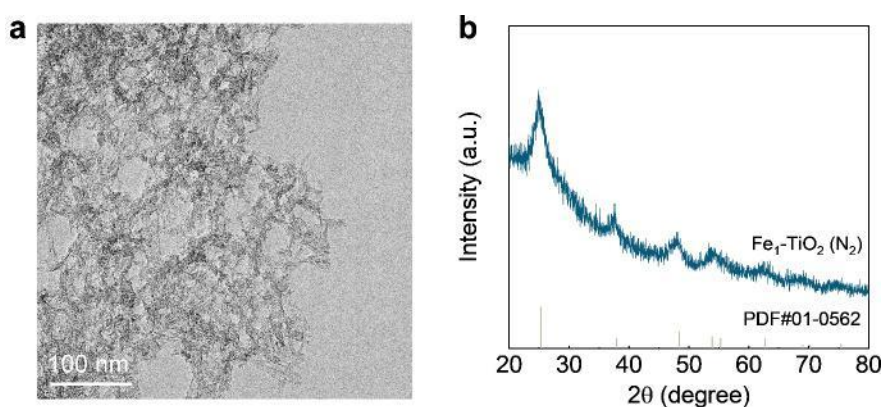

Fig. R18. (a) TEM image and (b) XRD pattern of Fe_1-TiO_2 nanostructures synthesized in N_2.

3. The authors should clarify how they determined the valence state of elemental Fe in Fe_1-TiO_2 nanostructures using the absorption edge position in X-ray Absorption Near Edge Structure (XANES) spectroscopy. A detailed explanation of any linear correlation observed would enhance the reader's understanding.

Response: We appreciate the reviewer's comment regarding our use of XANES spectroscopy at the Fe K-edge to assess changes in the valence state. This technique measures the shift in the absorption edge position, which correlates with the energy required to excite an electron from a core level to an unoccupied state. This shift is indicative of the oxidation state of the absorbing atom and is instrumental in identifying changes in the valence state. Typically, a shift toward higher energies signifies a higher oxidation state, while a shift toward lower energies indicates a lower oxidation state. By comparing the observed absorption edge position with reference spectra from known Fe oxidation states—such as Fe metal (Fe^0), Fe_3O_4 (Fe^{2+}, Fe^{3+}), and Fe_2O_3 (Fe^{3+})—we can ascertain the oxidation state of Fe within the Fe_1-TiO_2 nanostructures.

Theoretically, valence is directly proportional to the energy of the absorption edge, and a linear relationship is established by analyzing standard samples across various valence states. The peak's absorption edge data are then integrated into this equation to calculate the valence. However, in practice, valence values derived from XANES can deviate from actual valence due to factors like the

atom's local environment, the energy resolution of the instrumentation, and potential data analysis artifacts. Consequently, specific valence values are not reported in our manuscript. Instead, we utilize XANES to provide insightful observations into the electronic structure and oxidation state trends within the materials under study.

4. In the production of Fe_1-TiO_2 catalysts, diethylene glycol (DEG) plays a crucial role. Typically, DEG ligands on the catalyst surface might hinder catalytic activity by blocking active sites or altering surface characteristics. This study takes a novel approach by retaining the DEG ligands, yet the catalyst exhibits excellent performance in photothermal catalysis for polyester up-cycling. The specific reasons for this effectiveness should be thoroughly explained.

Response: Thank you for your insightful question. In the photothermal catalytic reaction for polyester upcycling, when the Fe_1-TiO_2 catalysts are exposed to simulated sunlight, they are excited by high-energy UV photons. This excitation leads to the generation of electron-hole pairs. The DEG ligand on the catalyst's surface effectively captures the holes, thus extending the electron lifetime by preventing rapid carrier recombination (*Angew. Chem. Int. Ed. 2023, 135, e202308930*). Following UV irradiation, there is a significant decrease in the photoluminescence intensity of the Fe_1-TiO_2 catalysts, as illustrated in **Fig. R19a**. This decrease is attributed to the catalyst's black color in its active state, which harbors abundant defect energy levels. These defects facilitate non-radiative carrier relaxation when the excitation light interacts with the catalyst's surface, leading to diminished fluorescence intensity. Further, the absorption spectrum reveals enhanced absorption of visible light, corroborating this observation. Moreover, the longevity of the electrons aids in the reduction of Ti^{4+} within the Fe_1-TiO_2 catalysts to Ti^{3+} species, simultaneously generating oxygen vacancies. As demonstrated in **Fig. R19b**, there is a dramatic increase in the count of Ti^{3+} and oxygen vacancies in the EPR spectra post-UV irradiation. This finding suggests that the photogenerated carriers interact primarily with the Fe_1-TiO_2 catalyst itself. The in-situ formed oxygen vacancies serve as catalytic sites that facilitate the adsorption and activation of C-O and C=O bonds in the PET carbon backbone, ultimately leading to exceptional catalytic performance.
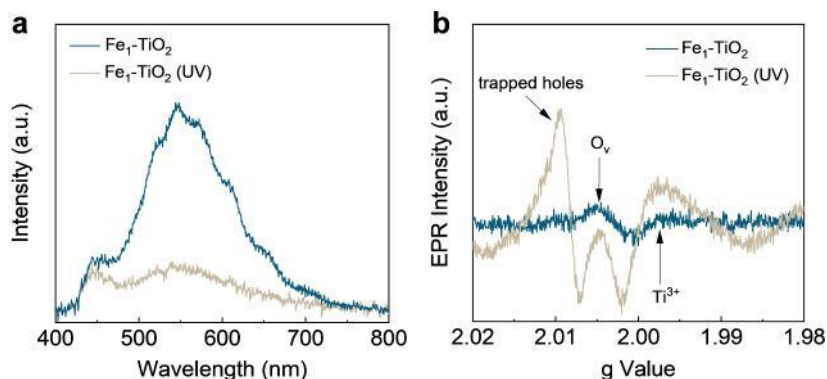

Fig. R19. (a) Photoluminescence and (b) EPR spectra of Fe_1-TiO_2 nanostructures before and after UV exposure for 30 min.

5. Evaluating the performance of the Fe_1-TiO_2 catalysts in photothermally catalyzed polyester upcycling is crucial. The authors should provide a comparison with other reported works and also describe the stability and morphology of the catalyst post-reaction.

Response: Thank you for your valuable comments. We have compared the Fe_1-TiO_2 catalysts with other catalytic systems previously reported for the glycolysis of PET, as detailed in **Table R3**. It is apparent from the data that under similar reaction conditions, the Fe_1-TiO_2 catalysts demonstrate superior space-time yields (STY).

Table R3. Comparison of catalytic performance of reported catalysts for the glycolysis of PET.

Catalyst	Catalyst amount (g)	PET (g)	Time (h)	BHET Yield (%)	STY @ 190 ^{oC} ($g_{BHET} \cdot g_{Cat.}^{-1} \cdot h^{-1}$)
$Zn(Ac)_2$	0.29	30	1	68.0	93.06
$ZnFe_2O_4$	0.20	5	6	79.5	4.38
OPA@Fe_3O_4	0.048	0.48	1.5	91.0	8.03
Fe_3O_4@SiO_2@(mim)[$FeCl_4$]	0.015	0.1	24	50.0	0.18
Zinc plates	2	5	5	77.7	0.51
Zn-BDC	0.06	6	3	87.3	38.49
SiO_2-Fe_2O_3-NH_2SB NP	0.1	1	3	73.0	3.22
[Ch][OAc]	0.25	5	3	83.8	7.39
t-BuP_2	0.25	0.5	1.5	92.7	1.64
4Ti/SBA-15	0.05	0.4	3/4	87.2	12.30
Fe_3O_4-CP NPs	0.01	1	2	56.9	37.64
ZnO-Fe_3O_4 HMNAs	0.5	1.5	0.5	92.3	7.33
$Zn(OAc)_2$	0.5	1.5	1/12	83.0	38.75
MeONa	0.28	1	2	75.0	1.77
[HDBU]Im	0.25	5	2/3	78.9	31.16
Cyanamide	0.1	2	2.5	95.2	10.08
MAF-6	0.05	5	4	78.3	25.89
$ZnCl_2$	1	5	2	81.1	2.68
$CoCl_2$	1	5	2	72.7	2.40
Mo/ZnO	0.01	1	1	92.3	122.11
GCNC	0.05	2	0.5	75.0	79.38
[Bmim]HCO_3	0.1	2	2	71.2	9.42
1,3-DMU/$Zn(OAc)_2$	0.25	5	1/3	82.0	65.75
rGO/[TESPMI]$_2$$CoCl_4$	0.15	1	3	87.3	2.57
$NaHCO_3$	0.25	5	3	48.0	4.23
Fe_1-TiO_2 (This work)	0.02	0.5	1/4	76.2	**100.81**

We conducted a thorough characterization of the morphology and structure of the Fe_1-TiO_2

catalysts after a 25-hour reaction period. As depicted in **Fig. R20**, no distinct Fe species were detected in the XRD patterns. The distribution of Fe elements within the Fe_1-TiO_2 catalysts was uniform, as confirmed by EDS mapping. Moreover, Fourier-transform EXAFS analysis indicated that the Fe atoms were exclusively coordinated with oxygen atoms, evidenced by a prominent peak at approximately 1.57 Å, attributable to Fe-O bonding. Notably, no Fe-Fe peak was detected at approximately 2.18 Å, confirming that the Fe single atoms were maintained within the Fe_1-TiO_2 catalysts post-reaction (**Fig. R21**). These findings collectively affirm the exceptional stability of the Fe_1-TiO_2 nanostructures following the polyester upcycling reaction.
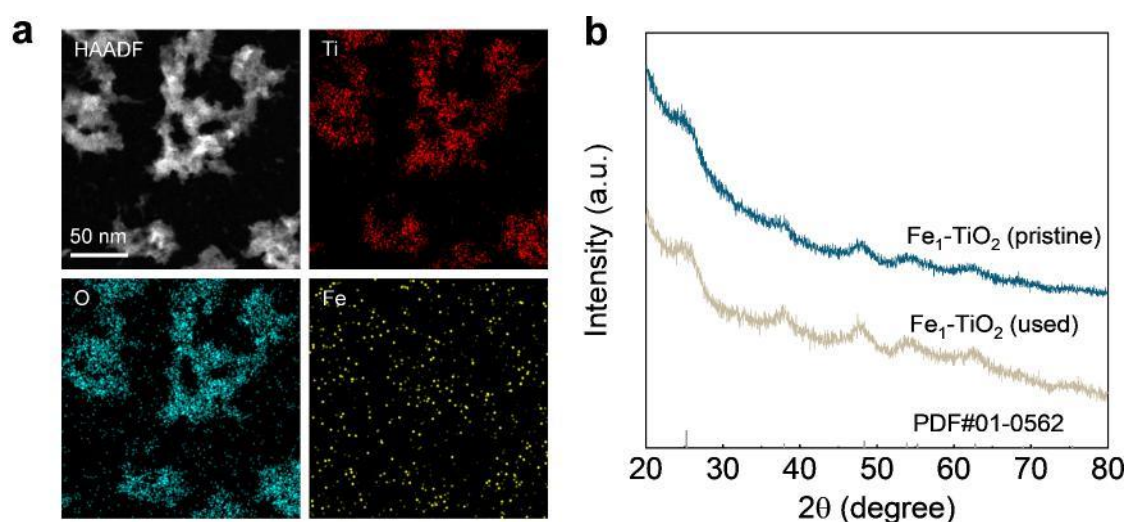

Fig. R20. (a) Elemental mappings and (b) XRD patterns of Fe_1-TiO_2 nanostructures after 25 h reaction.
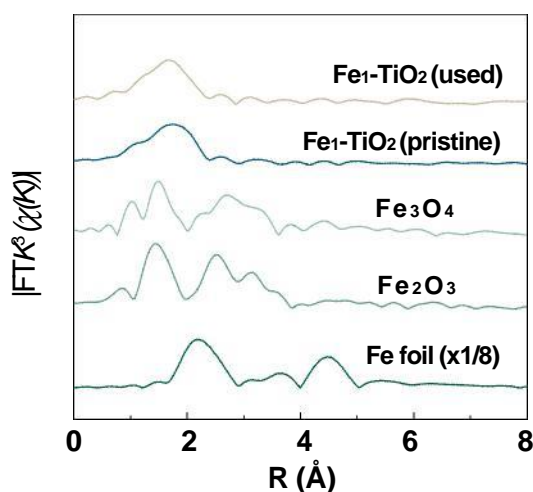

Fig. R21. Normalized FT-EXAFS spectra of pristine and used Fe_1-TiO_2.

6. It is advisable to specify the reaction conditions such as temperature, duration, and whether conditions are thermal or photothermal in the figure legends of both the manuscript and supplementary

information.

Response: Thank you for raising the question, and we apologize for the unclear description in the manuscript and supplementary information. Accordingly, we have revised the whole manuscript.

7. Detailed purity characterization data for the upcycled polyester product should be provided.

Response: Thanks for your valuable suggestions. We utilized the integration of the peaks in the [1H] NMR spectrum for product quantitative analysis. As shown in **Fig. R22a**, the single signal observed at ö 8.1 ppm corresponds to the four symmetric aromatic protons of the benzene ring. Additionally, the triplet peak at ö 4.3 ppm and the quartet peak at ö 3.7 ppm represent the methylene protons of COO-CH_2 and CH_2-OH, respectively. The triplet peak at ö 4.9 ppm indicates the presence of protons from the hydroxyl group. The peak area ratio of these peaks (2.01:0.99:1.99:2.00) aligns with the theoretical value (2.00:1.00:2.00:2.00), Furthermore., the FT-IR spectra of our products overlap well with commercial BHET (**Fig. R22b**), again suggesting the high purity of the product.
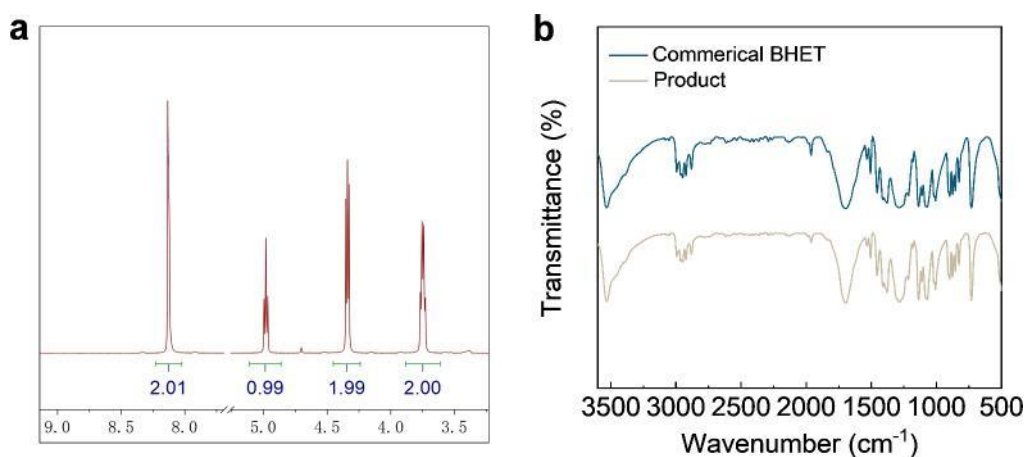

Figure R22. (a) [1H] NMR spectrum and (b) FT-IR spectrum of the recycled BHET.

RESPONSE TO REVIEWERS' COMMENTS

Reviewer #1:

The authors have addressed the issues raised, however, some of the current formulations as well as the innovations are not convincing before considering this MS to be accepted. The detail suggestions are as following:

Response: Thank you very much for your detailed and constructive feedback on our manuscript. We appreciate the time and effort you have taken to review our work thoroughly. We understand your concerns regarding the current formulations and innovations presented in the manuscript. We are committed to addressing these issues comprehensively and have carefully considered each of your suggestions. We believe that these revisions have significantly strengthened the manuscript, and we hope they meet your expectations. We sincerely appreciate your critical insights, which have been instrumental in improving the quality of our work. Thank you once again for your valuable feedback.

1. The authors argue that the single-atom content is a summation of the bulk phase and the surface. There is no different from ordinary doping and has been studied extensively, so the innovativeness of the article needs further elucidation.

Response: We are grateful for the reviewer's insightful comments. Heteroatom doping has been used as a universal strategy to prepare a wide range of single-atom catalysts. However, conventional doping methods still face significant challenges in scalable synthesis of M_1-TiO_2 with high doping concentrations, which mainly arise from the fact that the accumulation of lattice strains becomes more pronounced with the increase of M_{hetero} concentration, thus hindering the formation of the M_1-TiO_2. Our proposed strategy combines the control of growth kinetics (using diethylene glycol DEG to passivate the hydrolytic activity of heteroatoms) and thermodynamics (releasing free energy from lattice mismatch through the introduction of a short-range ordered structure). This method provides a versatile and scalable synthetic platform for the creation of M_1-TiO_2 nanostructures with high heteroatom concentrations.

Importantly, in M_1-TiO_2 catalysts prepared by conventional doping systems, the heteroatoms are uniformly distributed within the TiO_2 matrix, which loses many reaction sites. In contrast, our proposed growth strategy based on kinetic difference control can construct a structure rich in heteroatoms on the surface, which improves the density of catalytic sites. To prove the above point, we analyzed the distribution of heteroatoms using X-ray photoelectron spectroscopy (XPS) depth profile technique. XPS depth profiling uses an ion beam to etch surface layers, revealing structural information at different depths. As shown in **Fig.R1**, the Fe-Ti atomic ratio on the catalyst surface is 13.7%, which decreases with the increase of etching depth. The Fe-Ti atomic ratio decreases to 7.8% when the etching depth is ~3 nm. These results confirm the ability of this technique to prepare M_1-TiO_2 catalysts with a surface rich in heteroatoms.

In summary, to address the challenges associated with traditional methods of synthesizing high-

load single-atom catalysts, we have developed a DEG-assisted approach. This method leverages principles of crystal growth kinetics and crystal thermodynamics to prepare a series of single-atom catalysts. Additionally, our approach facilitates the synthesis of structures enriched with surface heteroatoms, providing a valuable complement to existing synthesis methods. We have incorporated these advancements into the main text in response to your suggestions, and we hope that our revisions meet your expectations.
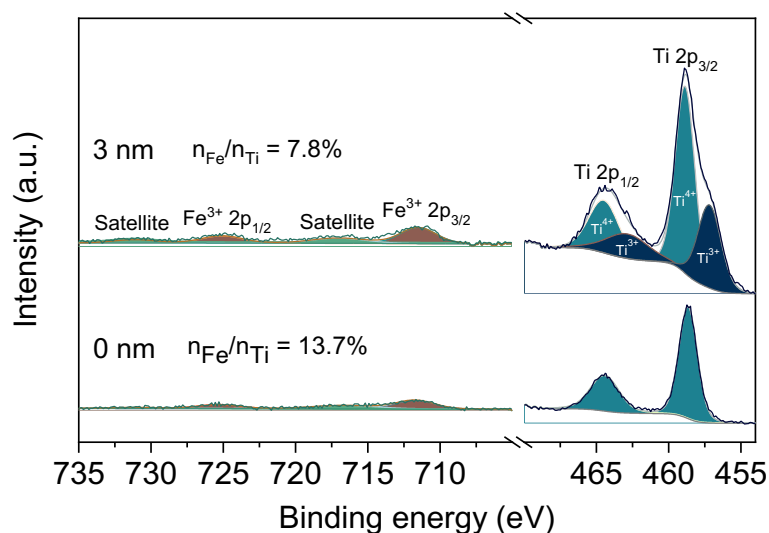

Fig. R1 Depth-dependent high-resolution Fe 2p and Ti 2p XPS spectra of Fe_1-TiO_2.

2. It is generally accepted that catalytic reactions are surface reactions, therefore accurate quantification of surface-active sites is important and the authors are advised to supplement the surface Fe content.

Response: We agree with the reviewer that surface active sites are important for catalytic reactions. To quantify the density of active adsorption sites on the catalysts surface. CO-temperature-programmed desorption (CO-TPD) is commonly used. However, the decomposition of the chemoadsorbed diethylene glycol (DEG) ligands interfered the TPD test. As shown in **Fig. R2**, DEG decomposition started at 250 °C and was complete at 650 °C, aligning with the thermogravimetric analysis (TGA) results. During this process, the decomposition of DEG generates a substantial gas, which interferes with the CO-TPD results, thereby impeding the technique's ability to accurately ascertain the surface Fe content. Hence, XPS was used to probe the near-surface Fe content of the catalysts. As shown in **Fig.R1**, the XPS depth profile technique showed that the Fe-Ti atomic ratio on the catalyst surface was 13.7%.
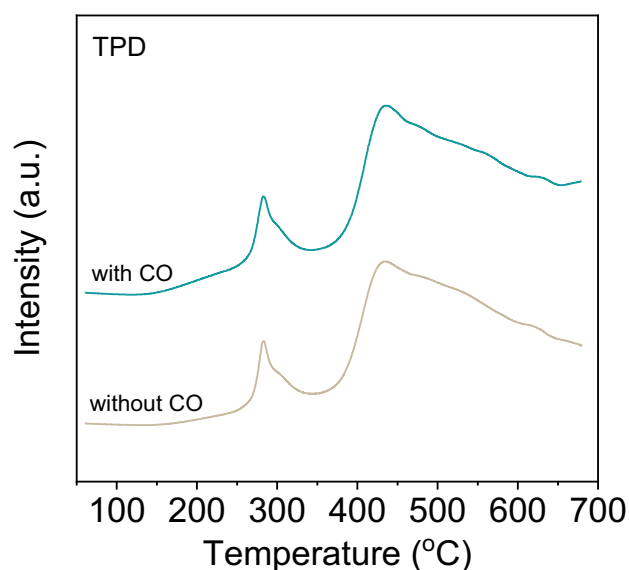
Fig. R2 CO-TPD curves of Fe$_1$-TiO$_2$.

3. In addition to considering the conversion rate, the by-products of the catalytic process as well as the selectivity should also be considered.

Response: We appreciate your constructive comment. Accordingly, we have conducted a thorough characterization of the products resulting from the catalytic process. Additionally, we have incorporated an analysis of BHET selectivity into the revised version of the manuscript. The BHET was quantitatively analyzed using ^{1}H NMR spectroscopy at 400-MHz Bruker AVANCE AV III instrument, with d^6-DMSO as the solution. The dichloromethane signals as internal standard (δ =5.76 ppm, 1H), and the representative characteristic signals areas for BHET (δ = 8.13 ppm, 4H) were calculated to determine the yield of the BHET in the ^{1}H NMR spectra (**Fig. R3**). The yield of BHET was calculated using the following equations:

$$n_{BHET} = \frac{A_{BHET}/N_{BHET}}{A_i/N_i} * n_i \tag{1}$$

$$Yield\ of\ BHET = \frac{n_{BHET}}{\frac{m_0}{M_{PET}}} * 100\% \tag{2}$$

where A_{BHET} and N_{BHET} refer to the characteristic signal peak area and protons number of BHET, respectively, A_i and N_i denote the characteristic signal peak area and the protons number of the internal standard, respectively, n_{BHET} and n_i refer to the mol of BHET and internal standard. m_0 represents the initial weight of PET; $M_{PET,}$ correspond to the molecular weight of PET repeating unit (192.2 g/mol).

In addition, the yield of BHET was further analyzed using a Dionex HPLC-U3000 equipped with a C18 column (5 μm, 250 × 4.6 mm^2, Agilent) and an ultraviolet detector set at 254 nm. The mobile phase, a mixture of methanol and water (v/v = 50/50) was run for a duration of 20 min at a temperature of 30 °C, with a flow rate of 0.4 mL min^{-1} and an injection volume of 15 μL. As shown in **Fig. R4**, the HPLC spectrum of our product is consistent with the commercial BHET peak positions and the product contains only a small amount of oligomers. Quantitative analyses revealed that the BHET yields obtained by HPLC were consistent with NMR results (**Fig. R5**).
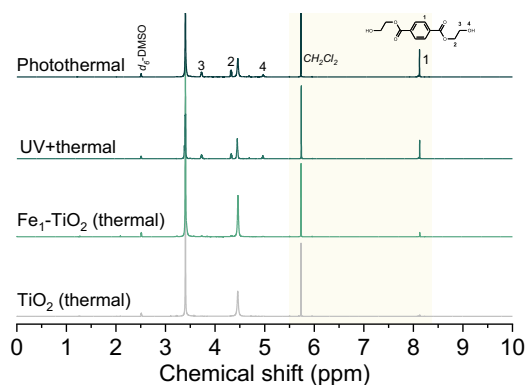

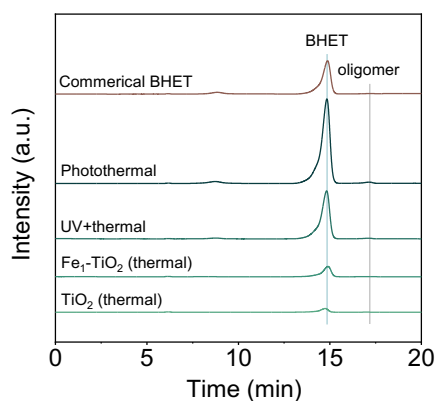**Fig. R3.** NMR spectrum of the recycled product at various conditions.

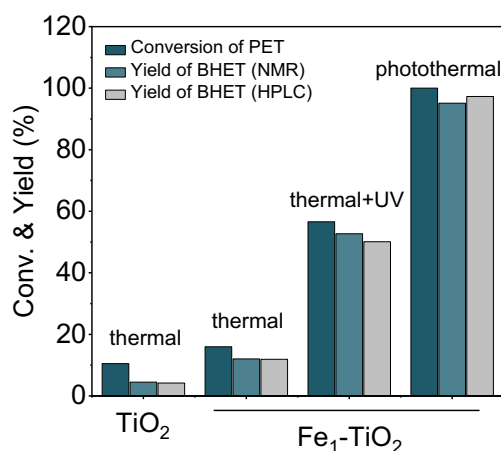**Fig. R4.** HPLC spectrum of the recycled product at various conditions.

Fig. R5 Glycolysis of PET catalyzed by Fe$_1$/TiO$_2$ and TiO$_2$ catalysts at various conditions.

4. In terms of activity, Fe does not show significant advantages over V, Co, Zn, Mo, etc.

Response: We appreciate the reviewer's thoughtful comments. The selection of the Fe_1-TiO_2 catalyst as an example was primarily based on two reasons. Firstly, during the catalyst screening, while the activity of the Fe_1-TiO_2 catalysts is comparable to these V, Co, Zn, and Mo-TiO_2 catalysts, its activity is in top-tier level. Additionally, Fe_1-TiO_2 catalysts have been widely applied in various significant research areas such as photocatalysis, environmental treatment, energy conversion, and organic synthesis. Achieving controllable preparation of this catalyst is expected to have direct applications in these fields.

Reviewer #2:

The manuscript improved a lot. Most of the questions were well addressed. It can be accepted.

Response: We extend our heartfelt thanks to you for your meticulous evaluation of our revised manuscript. Your insightful comments and constructive suggestions have been instrumental in enhancing the comprehensiveness, rigor, and persuasiveness of our study.

Reviewer #3:

In this revision, the authors gave more clarification by citing literature or using additional information on characterization and applications. The quality of this work is obviously improved. I suggest acceptance as it is.

Response: Thank you very much for your thorough review and positive feedback on our manuscript. We are delighted to hear that you find the quality of our work has improved and that the clarifications and additional information we provided have been helpful. We sincerely appreciate your suggestion to accept our manuscript as it is. Your constructive comments have been invaluable in enhancing the quality of our work, and we are grateful for your support throughout this process. Thank you once again for your time and effort in reviewing our work.

RESPONSE TO REVIEWERS' COMMENTS

Reviewer #1:

The author responded in detail to the questions we asked, and the current version is suitable to be accepted.

Response: Thank you very much for your thorough review and positive feedback on our manuscript. We sincerely appreciate your suggestion to accept our manuscript.